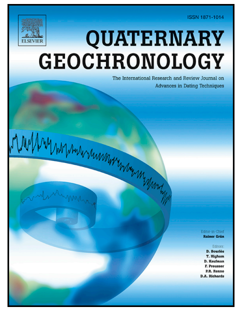

Investigation of OSL surface exposure dating to reconstruct post-LIA glacier fluctuation in the French Alps (Mer de Glace, Mont Blanc massif)

Benjamin Lehmann, Pierre G. Valla, Georgina E. King, Frédéric Herman

PII: S1871-1014(17)30112-7

DOI: 10.1016/j.quageo.2017.12.002

Reference: QUAGEO 882

To appear in: *Quaternary Geochronology*

Received Date: 7 July 2017

Revised Date: 23 November 2017

Accepted Date: 3 December 2017

Investigation of OSL surface exposure dating to reconstruct post-LIA glacier fluctuation in the French Alps (Mer de Glace, Mont Blanc massif)

Benjamin Lehmann[1], Pierre G. Valla[1,2], Georgina E. King[1,2] and Frédéric Herman[1]

[1] Institute of Earth Surface Dynamics, University of Lausanne, Lausanne, 1012, Switzerland
[2] Institute of Geological Sciences and Oeschger Centre for Climate Change Research, University of Bern, Bern, 3012, Switzerland

Correspondence to: Benjamin Lehmann (benjamin.lehmann@unil.ch)

Abstract

Providing quantitative constraints on late Pleistocene glacier fluctuations remains an important challenge for understanding glacier response to past and future climate changes. In most mountainous settings, paleo-glacier reconstructions are limited because they often lack precise temporal constraint. Different geochronological methods have been developed and applied to date specific geomorphological or sedimentological markers for paleo-glacier dynamics. Recently, OSL (optically stimulated luminescence) surface exposure dating has been introduced and provides us with an opportunity to improve paleo-glacier reconstructions. This method is based on the sensitivity of the OSL signal from rock minerals to light, resulting in bleaching of the OSL signal within the upper first millimeters of the exposed rock surface, a process that depends on the exposure age, the rock type and the local setting (e.g. topographic shielding, bedrock orientation etc.). Here, we investigate the potential of OSL surface exposure along a vertical cross-section of polished bedrock surfaces with known post-LIA (Little Ice Age) exposure ages (from 3 to 137 years) along the Mer de Glace glacier (Mont Blanc massif, France). The infra-red stimulated luminescence (IRSL) signals from rock slices exhibit increasingly deep bleaching profiles with elevation and thus exposure age, which is consistent with progressive glacier thinning since the LIA. Our results show that OSL surface exposure dating can be applied to periglacial environments, and is a promising tool for high-resolution reconstruction of ice-extent fluctuations, both in space and time.

Keywords: Optically stimulated luminescence (OSL), surface exposure dating, luminescence depth profile, paleo-glacier reconstruction, Mont Blanc massif

1. Introduction

During the last ca. 5 Ma of the Earth's history, global climate cooled and evolved towards oscillating climatic conditions that intensified towards the present (e.g. Zachos et al., 2001; Herbert et al., 2016). This climate shift left a strong imprint on mountain topography (e.g. Penck, 1905; Broecker and Denton, 1990; Molnar and Engand, 1990; Peizhen et al., 2001; Egholm et al., 2009). However, understanding paleo-climatic conditions in mountainous areas over the Plio-Pleistocene epochs remains difficult. Local records of successive glacial/interglacial cycles are scarce or poorly preserved over such long timescales (Ehlers and Gibbard, 2007). Polar ice-sheets and marine cores are useful for providing long-term global climatic records but are unable to describe regional continental climate. In contrast, glaciers and their fluctuations through time provide invaluable information on past mountain climatic conditions. Through mapping and dating moraine deposits and erratic boulders, it is possible to reconstruct the history of ice-extent (e.g. for the European Alps: Ivy-Ochs et al., 2006; Bini et al., 2009; Preusser et al., 2011; Schimmelpfennig et al. 2014; Ivy-Ochs et al., 2015; Wirsig et al., 2016).

Past glacier extents in the European Alps are well constrained since the Little Ice Age (LIA: 15th to 19th centuries). Using historical maps, survey reports and aerial photogrammetry, glacier fluctuations have been precisely reconstructed over the last two centuries (e.g. Vincent et al., 2014). To go further back in time into the Pleistocene, different geochronological methods can be used such as lichenometry (Winkler et al., 2004), varve chronologies (Stewart et al., 2011), dendrochronology (Baillie, 1995) and radiocarbon dating (Hajdas, 2008). However, organic matter can be scarce for glacial/periglacial deposits because of extremely active geomorphic systems associated with glacial environments. In addition to these methods, surface exposure dating of polished bedrock or erratic boulders using terrestrial *in situ* cosmogenic nuclides has been developed over the last decades (Lal et al., 1991; Gosse and Philips, 2001; Balco, 2011; Ivy-Ochs and Briner, 2014), and has been widely used in the European Alps (see Ivy-Ochs et al., 2006; 2009 for reviews). The combination of different cosmogenic nuclide pairs (e.g. ^{10}Be and ^{14}C: e.g. Goehring et al., 2012; Hippe et al., 2014) provides us with important information on Alpine glacier paleogeography since the Last Glacial Maximum (LGM; Ivy-Ochs et al., 2006; Wirsig et al., 2016). However, the cosmogenic nuclide production rate and the integration of production over the first 1-2 meters below a rock surface may limit the resolution of such methods for recent and/or complex exposure histories.

Here we investigate whether optically stimulated luminescence (OSL) surface exposure dating can be used to reconstruct recent glacier fluctuation. Luminescence dating is based on the accumulation of trapped electrons through time in the crystalline lattice of certain minerals (e.g. quartz or feldspar). Some of these trapped electrons are sensitive to daylight exposure (Aitken, 1985; Huntley et al., 1985). Luminescence dating is commonly used to date sediment burial in a range of geomorphological environments (e.g. Duller, 2008; Rhodes, 2011; Fuchs and Owen, 2008) but can also be used to determine rates of bedrock cooling (Guralnik et al., 2015; King et al., 2016; Brown et al., 2017), and the exposure age of archaeological rock surfaces (Polikreti et al., 2003; Sohbati et al., 2011). This latter application is based on the principle that when a rock surface is exposed to light, the luminescence signal, which is initially homogenous within the rock sample (at a given level or in field steady-state; e.g. Valla et al., 2016), will progressively decrease at depth until being completely zeroed, a phenomenon called “bleaching” (Aitken, 1998). The assumption used in this study is that the longer a surface has been exposed to daylight, the deeper the signal bleaching will be (Polikreti et al., 2002). In granitic and gneissic rocks, bleaching through time has been shown to occur over the first few centimetres depth of the rock surface (Vafiadou et al., 2007; Sohbati et al., 2011; Freiesleben et al., 2015). In alpine environments, glacier advances during the late Pleistocene to Holocene have been associated with subglacial erosion of bedrock at the centimetre-scale (e.g. Goehring et al., 2011). This means that only the most recent exposure history of the bedrock will be recorded, as earlier exposure histories and OSL bleaching evidence will have been eroded by subsequent glacier advances. OSL surface exposure dating would thus in theory enable past glacier extents to be reconstructed with a high temporal resolution for both recent and complex exposure histories. Furthermore, this method is attractive because of the short time required for sample preparation (Sohbati et al., 2011), although one current disadvantage is the requirement for calibration of this chronometer on rock surfaces with independently known exposure ages (Sohbati et al., 2012a).

In the following, we first introduce the study site, i.e., the Mer de Glace, and our sampling strategy. We have targeted several independently dated glacially eroded bedrock surfaces, which represent past elevations of the glacier surface since the LIA. We then review the basic principles of the method and present the luminescence signals for six different surfaces along a vertical cross section above the present-day Mer de Glace. Our results show a strong correlation between sample elevation, exposure age and bleaching depth. Finally, we use this dataset to show that model calibration requires multiple samples of known age to take full advantage of OSL surface exposure dating in both glaciated and formerly glaciated environments.

2. Setting and sampling strategy

2.1. Geomorphological setting

The Mer de Glace glacier (Fig. 1) is about 11.5 km long and is located in the Mont Blanc massif. The modern glacier covers an area of 30.4 km^2 (excluding former tributary Talèfre Glacier) and spans an elevation range from 4205 m to 1531 m.a.s.l. (data from 2008; Gardent et al., 2014). The mean equilibrium line altitude (ELA), reconstructed using remote sensing methods, was about 2880 m.a.s.l. between 1961 and 1990 for five of the main north-facing Mont Blanc massif glaciers, including the Leschaux Glacier for the period 1984-2010 (Rabatel et al., 2013).

The Mer de Glace is an appropriate laboratory for validating the application of OSL surface exposure dating for paleo-glacier reconstruction. Numerous studies have provided detailed reconstructions of Mer de Glace fluctuations from the LGM towards the Holocene and present day (Coutterand and Buoncristiani, 2006; Nussbaumer et al, 2007; Vincent et al., 2014; LeRoy et al., 2015). The Montenvers site (Fig. 1) was chosen as an optimal study site as the evolution of the glacier thickness since the LIA has been reconstructed by Vincent et al. (2014) using historical maps, aerial photogrammetry and satellite-derived digital elevation models (see Section 2.3 for details). Furthermore, the rock type is generally homogenous along the valley flank (i.e. orthogneiss; Dobmeier et al., 1998), avoiding any lithological dependency of the OSL surface exposure dating approach although occasional granitic lenses are exposed in the lower part of the profile (see Section 2.2 for details).

Our sampling strategy was to collect glacially polished bedrock surfaces with the best-preserved erosion patterns (glacial striations, roches moutonnées; Fig. 3) to ensure that sample bleaching profiles reflect the period of time since post-LIA deglaciation. The samples were also selected to have low topographic shielding and vegetation cover (e.g. lichen). Steep slopes were selected (i.e. above 30°) to limit any potential snow cover effects. In particular, we focused on rock surfaces exhibiting striations parallel to the Mer de Glace flow line in order to avoid the potential influence of tributary glaciers.

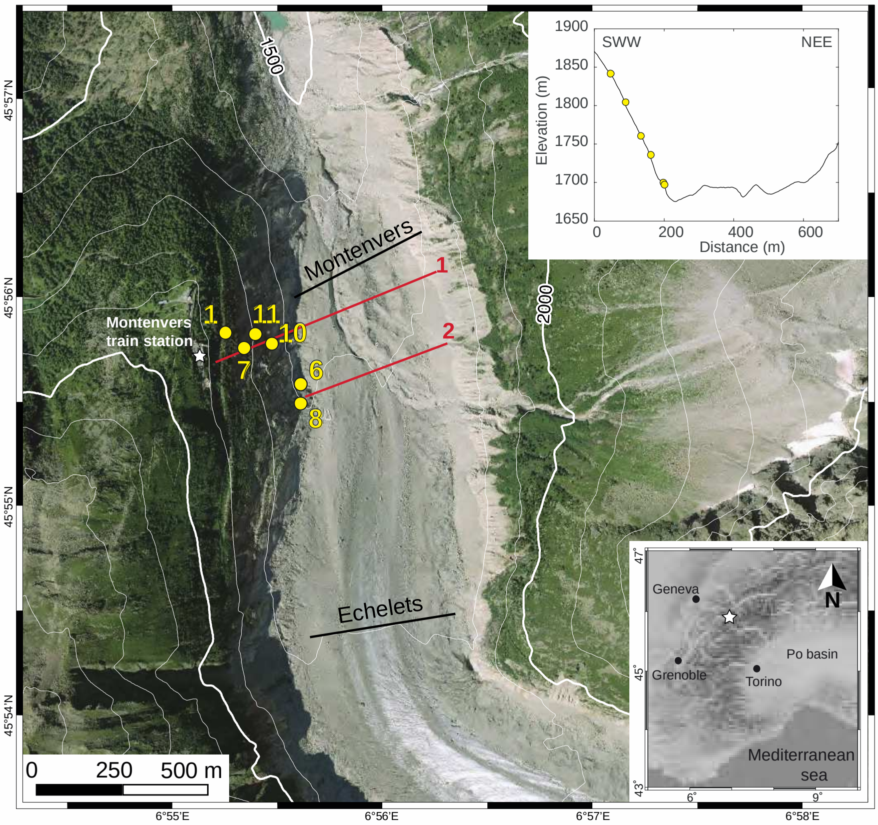

Figure 1: Sampling map of the Montenvers site, Mer de Glace. The orthorectified aerial photograph of the Mer de Glace was acquired in 2016 (source: www.geoportail.gouv.fr). The black lines show the two cross-sections produced by Vincent et al. (2014) which we interpolated to reconstruct glacier surface elevations at two different locations (red lines 1 and 2, see Section 2.3 and Supplementary Fig. A1) where samples were collected (yellow dots with numbers). Upper right inset represents the collected samples projected along cross-section 1. Bottom right inset shows location of the study area within the western Alps.

2.2 Sample description

We collected six samples along the Montenvers profile during several field campaigns (2015-2016), ranging in elevation from 1841 to 1696 m.a.s.l. (Fig. 1 and Table 1). Samples MBMV1, MBMV7, MBMV8, MBMV10 and MBMV11 consist of coarse-grained orthogneiss, typical for the Aiguilles Rouges massif (Dobmeier et al., 1998). These rocks mainly comprise coarse K-feldspar crystals, quartz, biotite and muscovite. Only MBMV6 was collected from a granitic lens, which consists of bigger quartz and feldspar crystals than the orthogneiss (Fig. 3b). Because differences in crystals properties may influence light penetration, i.e. due to both crystal size and distribution, sample MBMV6 is used to explore any potential lithological effect on the OSL surface exposure dating approach.

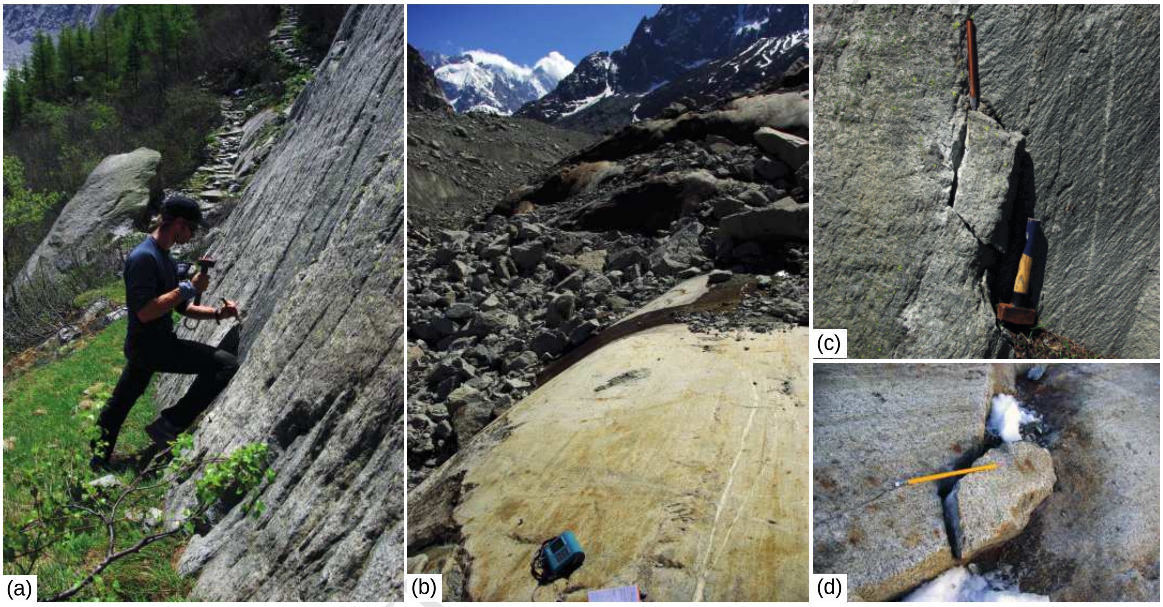

Figure 2: Sampling sites and sample details at the Montenvers site. (a-b) Sampling sites for MBMV7 and MBMV6. (c-d) Outcrops and samples MBMV7 and MBMV6.

Table 1: Sample characteristics from the Montenvers cross-section. Estimated exposure ages were reconstructed using differential GPS and ice-thickness reconstruction as shown in section 2.3. Shielding factors were calculated with the geometric shielding calculator (CRONUS-Earth project). Note that all estimated exposure ages are referenced from 2015 (date of the first field campaign).

Sample ID	Latitude	Longitude	Elevation	Lithology	Estimated Exposure Age	Topographic	Surface
	WGS 84		[m.a.s.l.]		[Year before 2015]	shielding factor	orientation
MBMV1	45°55'54.0"	06°55'07.7"	1841	Gneiss	137	0.81	N8 55°E
MBMV6	45°55'48.9"	06°55'17.7"	1696	Granite	2	0.92	N0 30°E
MBMV7	45°55'52.7"	06°55'09.9"	1804	Gneiss	69	0.79	N374 60°E
MBMV8	45°55'47.7"	06°55'18.5"	1699	Gneiss	3	0.81	N13 54°E
MBMV10	45°55'54.0"	06°55'14.1"	1735	Gneiss	18	0.79	N0 60°E
MBMV11	45°55'54.3"	06°55'11.5"	1760	Gneiss	30	0.88	N355 75°E

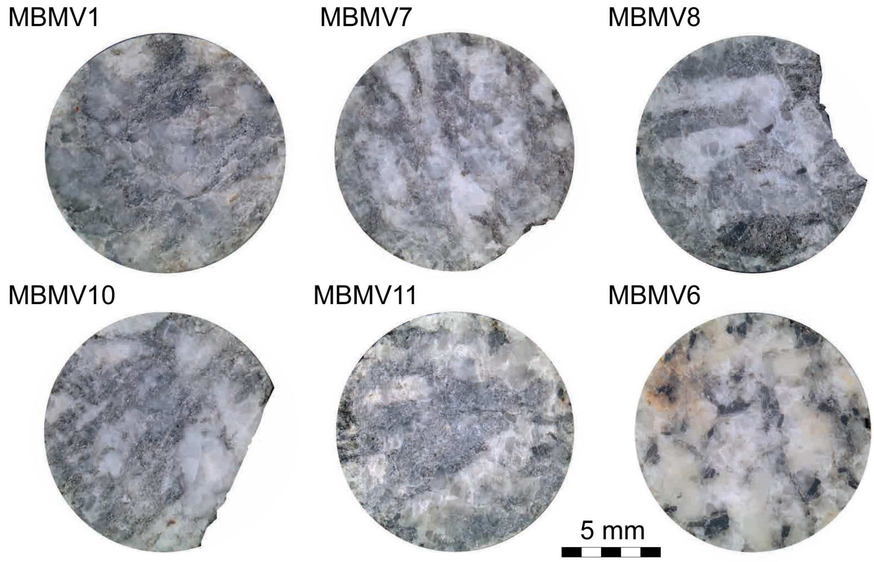

Figure 3: Pictures of selected rock slices (see section 3.1 for details), showing the difference in composition and texture between orthogneiss (MBMV1, MBMV7, MBMV8, MBMV10, and MBMV11) and granite (MBMV6).

2.3 Independent age calibration from glacier thickness reconstruction

We use the historical post-LIA reconstruction of the Mer de Glace thickness (Vincent et al., 2014) available for two cross-sections: Montenvers and Echelets (Fig. 1). Samples MBMV1, MBMV7, MBMV10 and MBMV11 were collected from the same profile located 290 m upstream of the Montenvers cross-section and 690 m downstream of the Echelets cross-section (cross-section 1, Figs. 1 and 4). Samples MBMV6 and MBMV8 were taken along a profile (cross-section 2, Fig. 1) located 200 m upstream of the cross-section 1. Because glacial thinning would progressively expose bedrock surfaces at lower elevations, we can use the relationship between exposure age and sample elevation to constrain the temporal evolution of glacial thickness (Fig. 1 and 4).

Post-LIA thickness reconstructions of the Mer de Glace for cross-sections 1 and 2 have been interpolated from the Montenvers and Echelets cross-sections. Exposure ages from 2 to 137 years were obtained for the different samples, using either cross-section 1 (MBMV1, MBV7, MBMV10 and MBMV11) or cross-section 2 (MBMV6 and MBMV8) (see Supplementary Material A1). All exposure ages are relative to the first sampling campaign in summer 2015.

3. Methodology: OSL surface exposure dating

3.1. Theoretical approach

Minerals such as quartz and feldspar naturally contain defects or impurities in their crystal lattice. Energy released by ambient radiation (i.e. cosmic rays and the flux of high-energy solar particles or/and radioactive decay in the rock-matrix) excites electrons from their equilibrium state (valence band), and these can become trapped at higher energy levels within the crystal. Because of the finite number of traps, electron filling occurs until saturation is reached. By giving energy to the system in the form of light or heat (natural bleaching processes), electrons are released and return to their equilibrium state, producing photons. This phenomenon is called luminescence and the intensity of a given luminescence signal is thus proportional to the number of trapped electrons (Aitken, 1985; 1998). In a rock surface continuously exposed to daylight, the progressive bleaching of the luminescence signal is expected to propagate deeper into the surface with time (Habermann et al., 2000; Polikreti et al., 2002; Laskaris and Liritzis, 2011).

Rock surface dating was first used in archaeology, and was based on thermally-stimulated measurements, i.e. thermoluminescence (TL; Liritzis et al., 1994; Richards et al., 1994; Theocaris et al., 1997; Polikreti et al., 2002; 2003). More recently, optically stimulated luminescence dating (OSL; e.g. Habermann et al. 2000; Vafiadou et al., 2007) has been introduced to date surface exposure, which benefits from improved measurement reproducibility and more rapid signal bleaching following exposure to daylight than typically-used TL signals (e.g. the 325°C TL peak in quartz). The potential of OSL for dating exposure events in geomorphological (Freiesleben et al., 2015; Sohbati et al., 2015) and archaeological (Liritzis, 2011) contexts has recently been investigated, and a range of applications including relative sea-level changes and coastal geomorphology (Simms et al., 2011; Simkims et al., 2013) have been published. However, OSL surface exposure dating has not yet been applied to glacially polished bedrock surfaces.

In mountainous environments, OSL dating can be used to evaluate the exposure age of a polished bedrock surface as described in Figure 4. At the initial condition (t_1 in Fig. 4), the glacier has reached its maximum thickness. Ice and periglacial sediments cover the bedrock surface, and the luminescence signals of bedrock minerals are in field steady-state and uniform in the rock column. When the glacier retreats, freshly-eroded surfaces are exposed to daylight (point **a** at time t_2, Fig. 4). The initial luminescence signals start to bleach for these exposed surfaces, while the sample at lower elevation is still covered by the glacier and its luminescence signals remain uniform in the rock (point **b** at time t_2, Fig. 4). As the glacier continues to thin, the lower part of the bedrock flanks are uncovered (t_3, Fig. 4) and the luminescence signals start to bleach for the lower-elevation surfaces. Therefore, in a setting affected by progressive glacier retreat and thinning, there is a direct correlation between the elevation of the studied site and the exposure age, with the assumption that the longer a surface is exposed to daylight, the deeper into the rock the luminescence signal is bleached (Freiesleben et al., 2015; Sohbati et al., 2011).

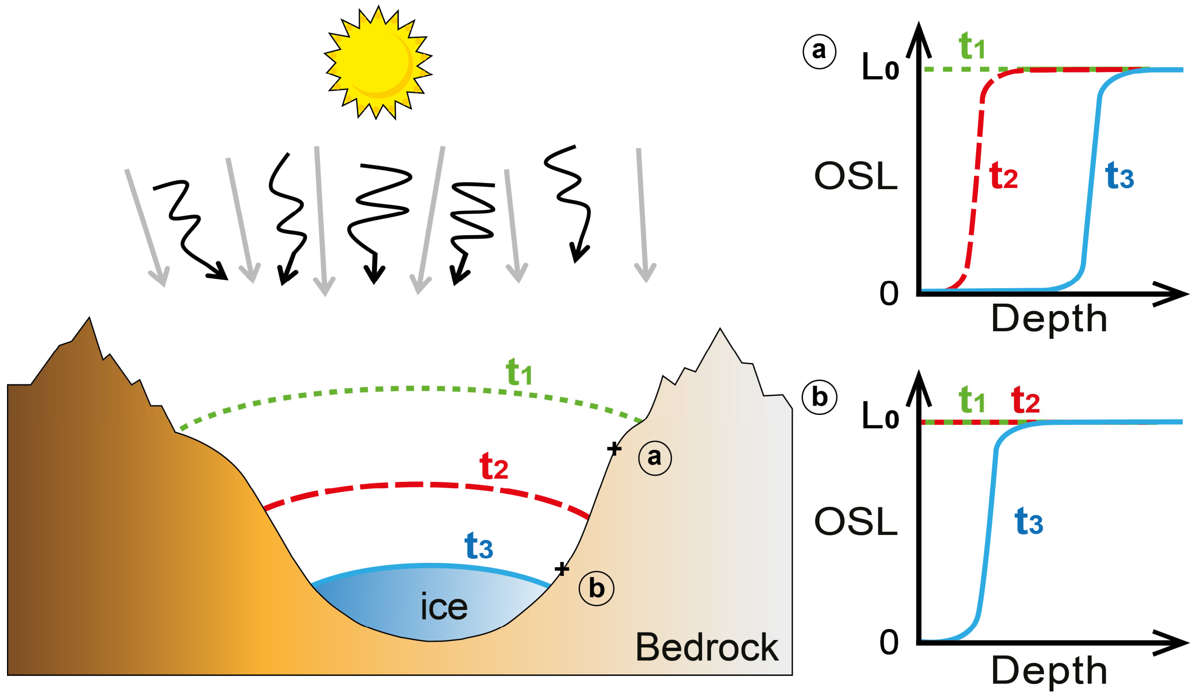

Figure 4: Sketch linking glacier thinning and OSL signal evolution for two bedrock surfaces located at different elevations along the valley flank. Straight arrows (grey) represent cosmic rays and high-energy solar particle flux; this radiation, together with radioactive decay in the rock matrix build up the latent luminescence signal. Other arrows (black) represent low energy electromagnetic radiation from the sun; this radiation bleaches the latent luminescence signal. At the initial time t_1, the glacier is at its maximum extent and the OSL signals for both surfaces are in field steady-state and uniform within the rocks, L_0. At time t_2, the glacier has retreated and exposed the surface (a), the OSL signal begins to bleach whilst surface (b) remains covered with its luminescence signal unchanged. In the final step t_3, the glacier size has shrunk, surface (a) remains exposed and its OSL signal is bleached at greater depth while surface (b) has just been exposed to daylight and its OSL signal has been bleached just below the exposed surface.

3.2. Modelling approach

To assess rock surface exposure durations to daylight from a luminescence depth profile, we use the model proposed by Sohbati et al. (2011; 2012a,b) who provide an in-depth review of each parameter. When a rock surface is exposed to daylight, both detrapping (due to the release of energy by daylight) and trapping (due to absorption of energy from ambient radiation) occur simultaneously. The trapped-charge concentration during light exposure is given by the following differential equation:

$$\frac{\partial n(x,t)}{\partial t} = -E(x)\,n(x,t) + F(x)\,[N(x) - n(x,t)] \qquad (1)$$

Where $n(x,t)$ is the trapped charge concentration [m^{-3}] at time t [s] and depth x [m], $N(x)$ is the concentration of sites [m^{-3}] available for trapping at depth x, $E(x)$ is the charge detrapping rate [s^{-1}], and $F(x)$ is the trap filling rate [s^{-1}]. The charge detrapping rate, *E(x)*, is itself given by:

$$E(x) = \overline{\sigma\varphi}_0 \, e^{-\mu x} \tag{2}$$

where $\varphi_0(\lambda, x)$ is the photon flux [cm^{-2} s^{-1}] describing the rate of incoming photons that can bleach the trap of interest. $\sigma(\lambda)$ is the photoionization cross section [cm^2] describing the probability of this specific trap to be excited by light stimulation. It is averaged over the wavelengths present in the solar spectrum at the surface ($x = 0$). Here, we assume that the photon flux does not fluctuate through time, and we are only concerned with the product of the two parameters, which is given by $\overline{\sigma\varphi}_0$ [s^{-1}] (i.e. the effective decay rate of luminescence; Sohbati et al., 2011). Equation (2) also includes a decay term for light attenuation with depth. The light attenuation coefficient μ [m^{-1}] describes how deep into the rock a photon will penetrate and affect the luminescence signal. μ is assumed to be independent of wavelength in the spectral range of interest (Sohbati et al., 2011).

For surface exposure dating of terrestrial surfaces, the effect of trap filling during daylight exposure over short timescales (i.e. centuries) is often negligible (i.e. $F(x) \approx 0$) (see Supplementary Material A2). The trapped charge population at a given depth (x) can then be approximated by:

$$n(x) = n_0 e^{-E(x)t} \tag{3}$$

where n_0 is the initial charge population [m^{-3}] assumed to be constant with depth within the rock column prior to bleaching. Assuming that the luminescence signal (L) is proportional to n, Eq. (3) becomes:

$$L = \frac{Lx}{Tx} = L_0 \, e^{-\overline{\sigma\varphi}_0 t \, e^{-\mu x}} \tag{4}$$

where Lx/Tx is the normalized natural luminescence signal measured at depth x [m] after exposure age *t* [s]. L_0 is the normalized natural luminescence signal before bleaching (Fig. 4), which is sample dependent and can be constrained in the laboratory.

Equation 4 can predict the rock luminescence profiles for different exposure ages, however the mean photon flux φ_0, the photoionization cross-section σ, and the attenuation coefficient μ must first be quantified. φ_0 is mainly controlled by the latitude and the cloudiness; and it is broadly correlated to elevation (Blumthaler et al., 1997). The solar irradiance is fluctuating over decadal timescales (Lean, 1987) making the independent determination of the photon flux impossible without knowing the time of exposure. The photoionization cross-section σ is depending on both the mineral and the trap targeted (Bailey, 2004). For samples coming from the same region and from a similar lithology, $\overline{\sigma\varphi}_0$ is assumed to be uniform and μ is expected to be of the same order of magnitude between samples, but not necessarily equal.

The OSL-depth profile of exposed rock surfaces with independently constrained exposure durations can be used to calibrate the $\overline{\sigma\varphi}_0$ and μ parameters by fitting the luminescence signal bleaching with depth (Singarayer, 2002; Sohbati et al., 2012a). These constrained parameters can then be used to determine the exposure histories of unknown-age surfaces from the same region.

Here, our objective is to demonstrate the validity of the proposed model (Eq. 4) on polished bedrock surfaces and to calibrate the model parameters on surfaces with known exposure age. To do so, the unknown $\overline{\sigma\varphi}_0$ and μ parameters are inverted for each sample using a probability density function of the model parameters, given the observed OSL-depth profile data. This includes a least absolute deviation regression $\mathcal{L}_{sample}$ (Eq. 5), in which we randomly prescribed a range of different $\overline{\sigma\varphi}_0$ and μ values. From the residual likelihood $\mathcal{L}_{sample}$ obtained, we select the maximum likelihood values of $\overline{\sigma\varphi}_0$ and μ. The modelled luminescence signals $\left(\frac{Lx}{Tx}\right)_m$ are calculated for each rock slice of a given sample using the known exposure age of each sampling site, giving:

$$\mathcal{L}_{sample} = \exp\left(-\frac{1}{2a}\sum_{i=1}^{n}\left|\left(\frac{Lx}{Tx}\right)_{obs}^{(i)} - \left(\frac{Lx}{Tx}\right)_{m}^{(i)}\right|\right) \quad (5)$$

where n is the number of rock slices per sample, $\left(\frac{Lx}{Tx}\right)_{m}^{(i)}$ is the luminescence signal calculated using Eq. (4), $\left(\frac{Lx}{Tx}\right)_{obs}^{(i)}$ is experimentally measured for each rock slice i and a is the uncertainty. Given that the scatter of the plateau signal (L_0) for every independent sample is larger than the analytical error, we use the standard deviation around the plateau value L_0 to estimate a. Then, we compute the combined likelihood for a number of samples p using:

$$\mathcal{L}_{combined} = \prod_{j=1}^{p} \mathcal{L}_{sample(j)} \quad (6)$$

This approach provides the most likely common values of $\overline{\sigma\varphi}_0$ and μ. Once the parameters of the model are determined as shown above, it is possible to invert the exposure age for other rock surfaces using the constrained $\overline{\sigma\varphi}_0$ and μ values (cf. Eq. (5)).

Table 2: Summary of symbols.

Symbol	Unit	Definition
n	m^{-3}	Concentration of trapped charge
x	m	Depth
t	s	Time
N	m^{-3}	Concentration of sites available too trap charge
E	s^{-1}	Charge detrapping rate due to solar radiation
F	s^{-1}	Charge trapping due to ionising radiation
σ	cm^2	Photionisation cross-section
φ	$cm^{-2}\ s^{-1}$	Photon flux
$\overline{\sigma\varphi_0}$	s^{-1}	Charge detrapping rate
μ	m^{-1}	Attenuation coefficient
Lx	Counts	Regenerated luminescence signal
Tx	Counts	Test dose signal
L	Counts	Luminescence

In order to verify our modelling approach, we show a synthetic inversion. We produce a synthetic luminescence signal ($\mathrm{Lx/Tx}$ for depths in between 0 and 14 mm) using Eq. (4) and sample-specific $\overline{\sigma\varphi_0}$ and μ parameters (obtained from initially fitting every sample using their independent age control, see Section 5.2 for details) and assuming a constant μ value (i.e. homogenous lithology with rock depth). The first step of the synthetic test is to invert parameters $\overline{\sigma\varphi_0}$ and μ knowing the exposure age t for each individual sample as presented above. Then, using these $\overline{\sigma\varphi_0}$ and μ parameters, we subsequently invert for the exposure age t using Eq. (4). In order to study the effect of potential uncertainties from the experimental data on the exposure age determination, we reproduce this synthetic test with white noise on the luminescence signal, with four different amplitudes between 0 and 100 % (Fig. 5). Our synthetic results show that our inversion approach can recover the exposure age with 0 to 50% noise. The synthetic test with 100% noise on the luminescence signal provided age outcomes with larger uncertainties (>20%). The best results are obtained using the best-fit of $\overline{\sigma\varphi_0}$ and μ and the median value of the predicted exposure ages. The resulting uncertainties are correlated with the magnitude of the noise, however any potential variability in the luminescence signal does not appear to produce a significant bias on the inverted exposure age.

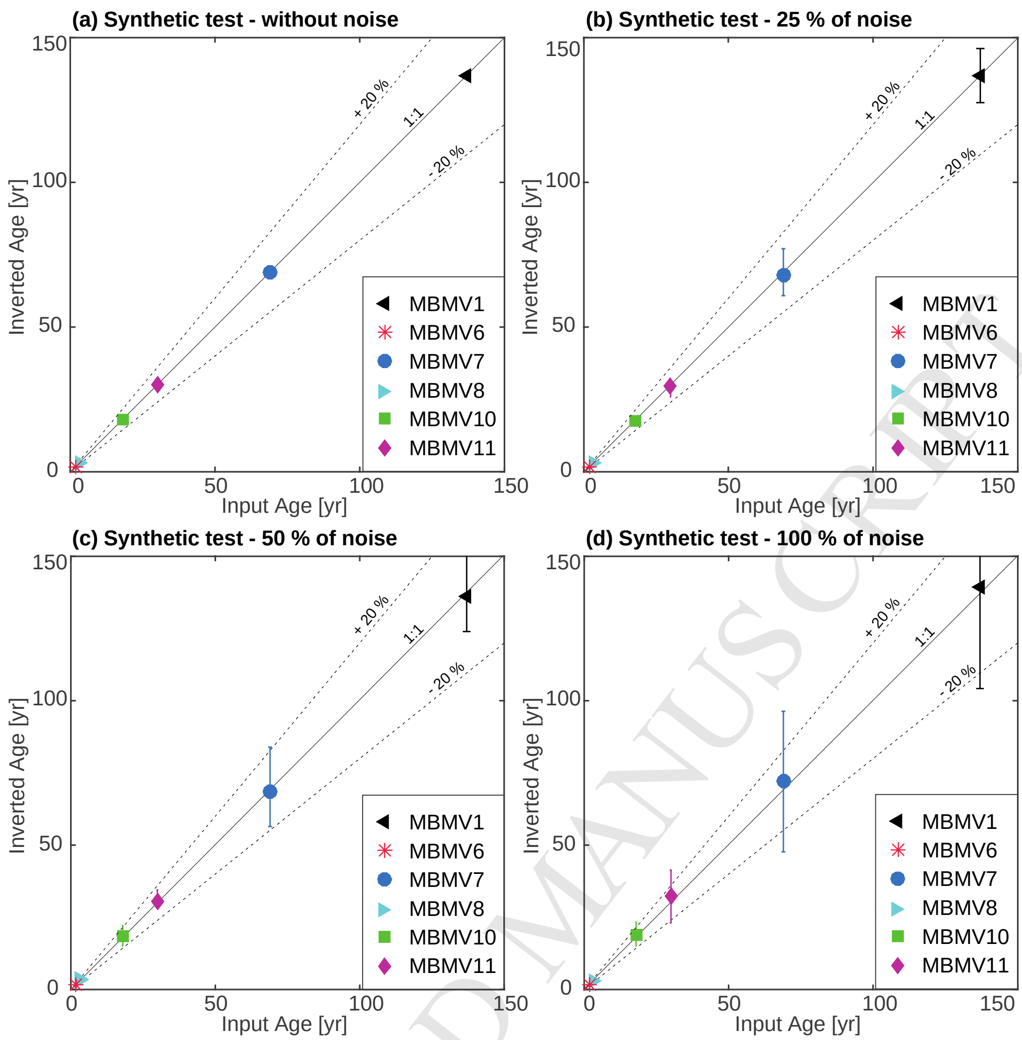

Figure 5: Results (median value) of inverted exposure age from the synthetic test, (a) without noise on the luminescence signal, (b) with 25%, (c) 50%, and (d) 100% noise. Error bars represent ±2σ on the inverted age.

4. Sample preparation and analysis

The bedrock samples were cored to 30 mm depth using a Husqvarna DM220 drill, with 10-mm diameter. Cores were then sliced into 0.7-mm thick rock slices with a BUEHLER IsoMet low speed saw equipped with a 0.3-mm thick diamond blade. The samples were drilled and sliced under wet conditions (water and lubricant, respectively) to avoid any heating that could potentially reset the OSL signal. Sample preparation was done under subdued red light conditions. The thickness of each rock slice was measured to determine the precise depth of each luminescence measurement.

All luminescence measurements were performed using Risø TL-DA 20 TL/OSL luminescence readers (Bøtter-Jensen et al., 2010) equipped with ^{90}Sr beta sources at the University of Lausanne (Switzerland). The readers have dose rates of ~0.1 and ~0.2 Gy s^{-1} and measurement reproducibility of 1.14 % and 1.26 % respectively. We first perform a preheat at 250 °C before giving infrared (IR) stimulation (870 nm, FWHM 40 nm) at 50 °C. Luminescence signals are detected through a filter combination of a Schott BG-3 and Schott BG-39. A uniform test dose was used (27.2 Gy) to measure the subsequent luminescence response (T_x) and to normalize the natural infrared stimulated luminescence (IRSL) signal (L_x) for every rock slice. Infrared stimulated luminescence was measured for 200 s and signals were integrated over the first 6 seconds whereas the background signal was integrated between 70-100 seconds. Measurements were analysed using Analyst v.3.22b (Duller, 2005). All thermal treatments and stimulations at temperatures greater than 200°C (i.e. preheat step) were carried out in nitrogen atmosphere. The experimental approach was validated using a dose recovery and preheat plateau test (see Supplementary Material A3; Murray and Wintle, 2000; Wintle and Murray, 2006).

5. Results

5.1. Experimental results

Figure 6 shows the luminescence measurements for representative samples MBMV1 and MBMV10 (results of the others samples are presented in Fig. 8). Three replicates (i.e. individual cores) per sample were sliced in a way that a depth and an IRSL signal can be attributed to each rock slice (unique colour/symbol for each individual rock slice in Fig. 6). The results show similar behaviour between the different cores for a given sample (Fig. 6). The IRSL signal is bleached near the surface and reaches a plateau at depth. Furthermore, and more importantly, the transition from a bleached signal to the plateau varies with the exposure age. The three core measurements reproduce well for both samples illustrated in Figure 6, with the mean standard deviation between the three cores ranging from 7 to 27% for all the studied samples. These results confirm experimentally that cores extracted from one individual sample record the same exposure history, supporting the proposed approach.

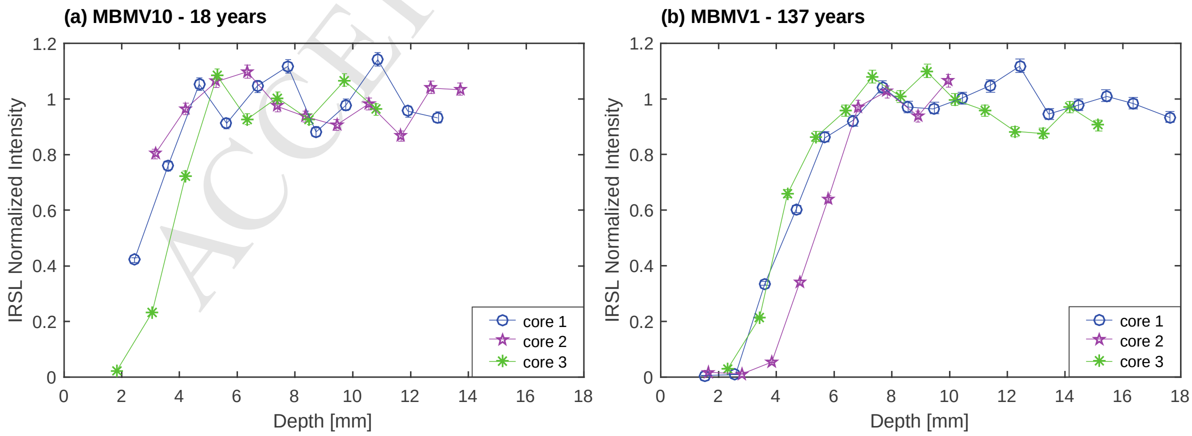

Figure 6: Infrared stimulated luminescence (IRSL) signal with depth for samples (a) MBMV10 and (b) MBMV1. Each coloured data point represents an individual rock slice. IRSL signals were normalized by L_0, which was determined by taking the average of the luminescence measurements

along the plateau. The plateau was defined when the luminescence signal is fluctuating by less than 20%.

5.2. Independent parameter determination

In this section, we determine the $\overline{\sigma\varphi_0}$ and μ parameters individually for each sample in order to study their potential variability from one rock surface to another (Table 3). As explained in Section 3.2, bedrock surfaces from the same location should share a common $\overline{\sigma\varphi_0}$ parameter (i.e. same order of magnitude; Blumthaler et al., 1997). Similarly, we expect that the μ parameter should be similar for samples from a uniform lithology. The determined parameters are then used in the inversion of the exposure ages for each sample individually (see Section 5.5). All inversion outcomes are summarized in Table 3. Samples MBMV1, MBMV8, MBMV10 and MBMV11 share similar effective decay rates ($\overline{\sigma\varphi_0}$) with the same order of magnitude (from 1.4 10^{-8} to 2. 10^{-7} s^{-1}) and show attenuation coefficients (μ) between 1.07 and 1.89 mm^{-1}. Samples MBMV6 and MBMV7 behave differently with much lower effective decay rates ($\overline{\sigma\varphi_0}$ of 2.0 10^{-6} and 4.2 10^{-6} s^{-1}, respectively), and different attenuation coefficients (μ of 0.92 and 2.50 mm^{-1}, respectively).

5.3. Parameter determination from joint probability estimates

We evaluate now the parameter determination from joint probability estimates in order to illustrate the benefit of having several known-age calibration samples. Figure 7a presents modelled results for sample MBMV10, which is representative of the other samples (except MBMV6 and MBMV7, see Section 5.2). The results show that log ($\overline{\sigma\varphi_0}$) and μ co-vary, which we attribute to measurement uncertainties and variability between the different cores. Figure 7b shows the area of acceptable fits when all the gneissic samples are included (i.e. excluding the granitic sample MBMV6).

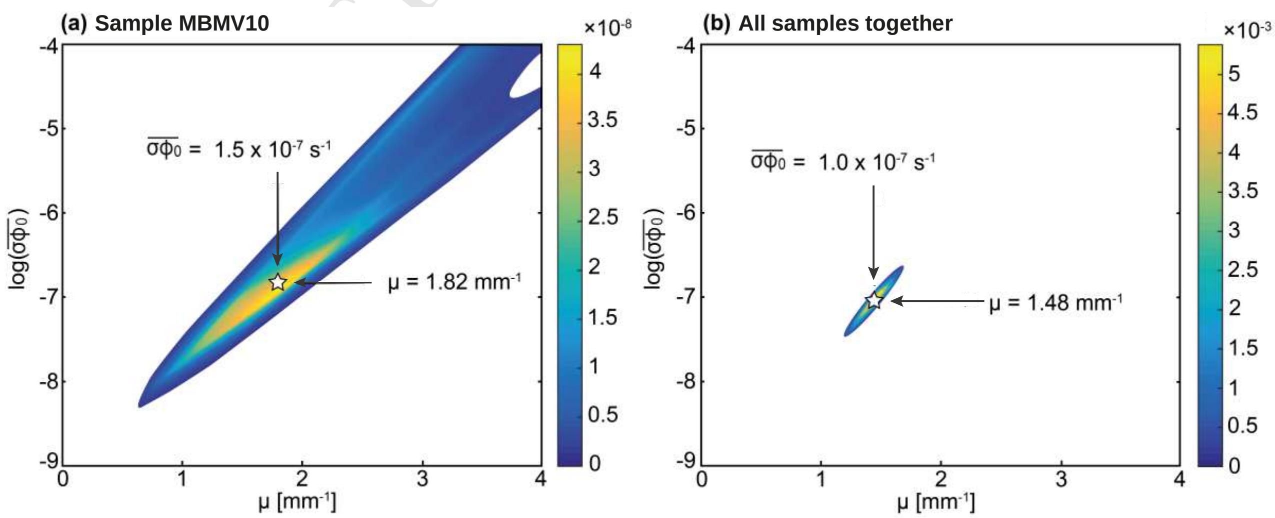

Figure 7: Relationship between the $\overline{\sigma\varphi}_0$ and μ parameters (a) for sample MBMV10, and (b) for all of the gneiss samples (i.e. excluding MBMV6) enabling determination of the shared $\overline{\sigma\varphi}_0$ and μ parameters (1.0 10^{-7} s^{-1} and 1.48 mm^{-1} respectively). For both figures, the colour scale shows the likelihood between modelled and experimental data (Eq. 6, note the differences in scaling between the two panels), and the star is the best-fit parameter values. Zero probability is not shown for clarity.

We then contrasted individual estimates of $\overline{\sigma\varphi}_0$ and μ for each sample, using different combinations of samples to estimate these parameters. The results are summarized in Tables 3 and A3. When inverting the model parameters with any combinations of three samples, all estimates of the effective decay rates are between 6.6 10^{-8} and 1.4 10^{-7} s^{-1}, and all estimates of the attenuation coefficients are between 1.33 and 1.57 mm^{-1}. Combinations of four samples provide $\overline{\sigma\varphi}_0$ values ranging from 7.2 10^{-8} to 1.2 10^{-7} s^{-1} and μ values between 1.38 and 1.53 mm^{-1}. According to Table 3 and Figure 7b, a common likelihood exists for all the gneissic samples calibrated together, giving an effective decay rate of 1.0 10^{-7} s^{-1} and an attenuation coefficient of 1.47 mm^{-1}.

Figure 8 depicts the normalized IRSL signals measured for all samples and their individually-constrained best-fit models (red lines) as described previously and illustrated in Figure 7a. The obtained outcomes show that the proposed model accurately describes the luminescence bleaching process through depth and time. The best-fit model calibrated with all of the gneissic samples together (black dashed lines, parameters in Table 3) fits close to the best-fit model determined for each sample individually (except MBMV6). These results confirm a key objective of the study, which is the possibility to calibrate the model parameters using different surfaces along a vertical profile, with the same lithology and different (independently-determined) exposure ages.

Table 3: Best-fit values of $\overline{\sigma\varphi}_0$ and μ determined for every sample individually and for all samples excluding MBMV6. Combinations of three or four samples are presented in Table A3 (Supplementary Material).

Parameter	$\overline{\sigma\varphi}_0$ [s^{-1}]			μ [mm^{-1}]		
Samples	Best-fit	+1σ	-1σ	Best-fit	+1σ	-1σ
Individually						
MBMV1	1.4 10^{-8}	1.5 10^{-8}	1.3 10^{-8}	1.07	1.08	1.05
MBMV6	2.0 10^{-6}	2.2 10^{-6}	1.8 10^{-6}	0.92	0.95	0.92
MBMV7	4.0 10^{-6}	5.0 10^{-6}	3.6 10^{-6}	2.52	2.56	2.46
MBMV8	2.2 10^{-7}	2.4 10^{-7}	1.5 10^{-7}	1.89	1.98	1.70
MBMV10	1.5 10^{-7}	1.5 10^{-7}	1.1 10^{-7}	1.82	1.87	1.75
MBMV11	4.2 10^{-8}	5.3 10^{-8}	3.9 10^{-8}	1.21	1.22	1.13
All samples together excluding MBMV6	1.0 10^{-7}	1.1 10^{-7}	9.5 10^{-8}	1.48	1.50	1.44

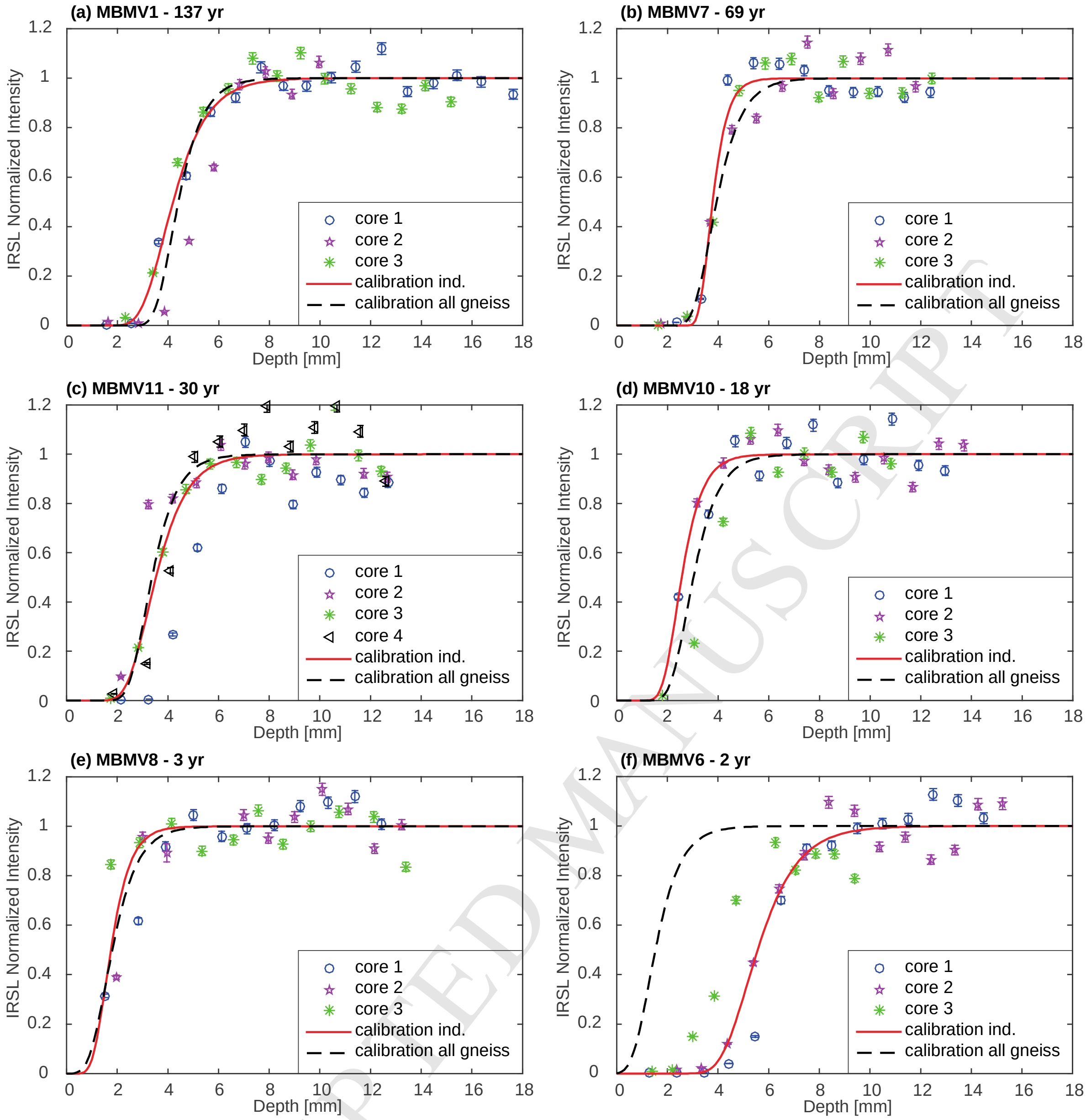

Figure 8: Normalized infrared stimulated luminescence (IRSL) profiles with depth and best-fit models. Coloured data point represents individual rock slice (each symbol/colour represents one core). The red lines show the best-fit model for each sample taken individually. The dashed black lines represent the best-fit model from a common calibration of the parameters using all gneiss samples together ($\overline{\sigma\varphi_0}$ = 1.0 10^{-7} s^{-1} and μ =1.48 mm^{-1}, cf. Fig. 7b and Table 3). Raw IRSL data are presented in Table A3(Supplementary Material).

5.4. Evolution of the luminescence signal through time

Compiling the best-fit models determined for each sample individually, a positive correlation between the exposure age and the depth at which the natural IRSL signal is zeroed can be clearly observed for samples within the same lithology (Fig. 9a). If we consider the inflection point of each individual model (Lx/Tx = 0.5 on Fig. 9a) as a proxy for the bleaching depth, this value ranges between 1.7 and

4.2 mm for 3 and 137 years of daylight exposure, respectively (Fig. 9b). The granitic sample MBMV6 does not follow this correlation, its bleaching depth being at 7 mm after 2-yr exposure to daylight.

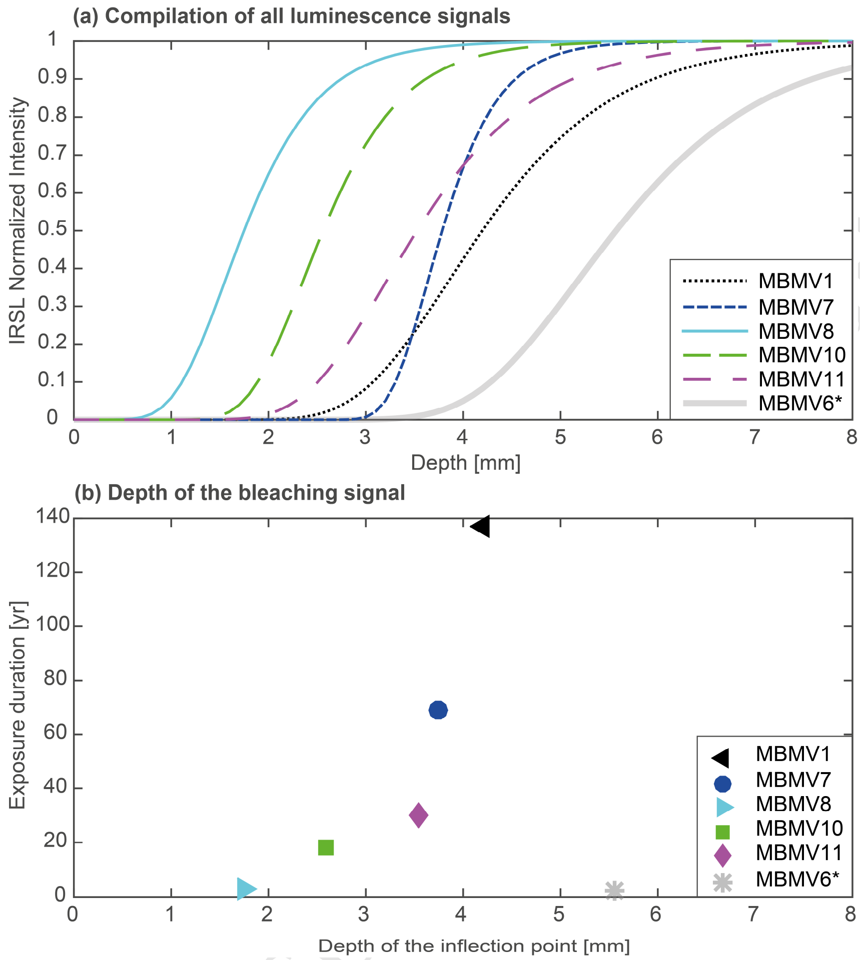

Figure 9: (a) Compilation of the best-fit models for each individual sample (cf. red lines in Fig. 8). (b) Correlation between the IRSL bleaching depth (i.e. the inflection point of the models presented in (a)) and the exposure age of each individual sample. The * symbol indicates the granitic sample (MBMV6); all the other samples are gneiss.

5.5. Inversion for exposure age

Once the model parameters have been determined by different sample combinations, it is possible to subsequently invert the exposure age as explained above. Figure 10 compares the exposure ages inverted from the different sample combinations, with the observed exposure age (all results are compiled in the Supplementary Table A4 and Figure A3). Figure 10a shows that our modelling approach is able to recover the observed exposure ages using parameters determined for each individual sample (<10% difference). When the exposure ages are inverted using the parameters determined for all of the gneissic samples together (as shown in Fig. 7b), there are slight differences between the inverted exposure age and independent age control (Fig. 10b, Table A4 and Figure A3).

The inverted ages are almost all within 20% of the observed ages except for sample MBMV11, which is overestimated by 90%.

Taking different calibration combinations with four (Fig. 10c) or three (Fig. 10d) samples also results in different performance regarding age predictions. For all gneissic samples, except MBMV11, the inverted exposure ages at 2σ are still within 20% of the observed ages. Note that in our approach the inverted exposure ages with four and three samples calibrations are only shown when the specific sample is not part of the calibration combination (grey shadow in the Supplementary Table A4). Although the match between the inverted and observed ages, as well as the trend between samples, is preserved independent of the calibration approach, our results show that the higher the number of calibration sites is, the better the inversion of exposure ages would be.

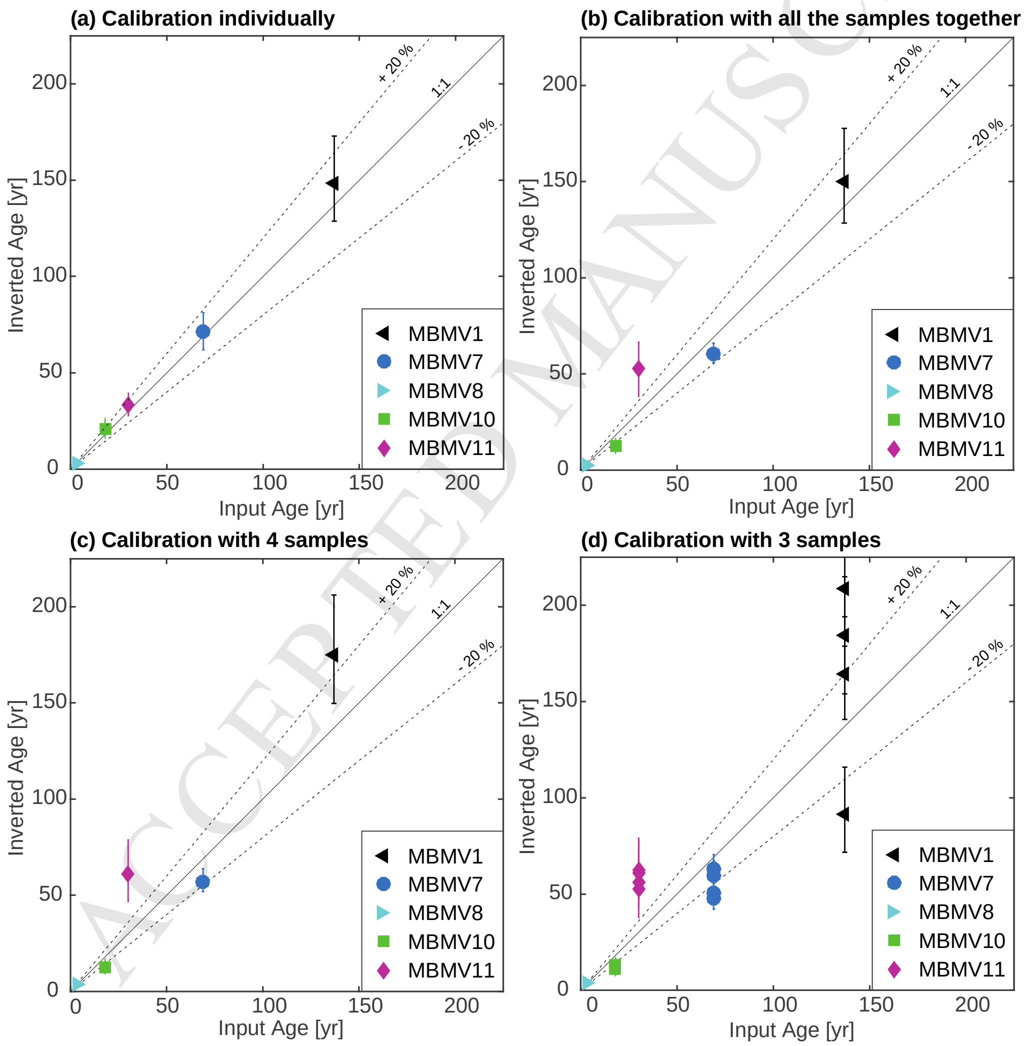

Figure 10: Correlation between inverted (median values) and observed exposure ages resulting from different calibration combinations to constrain the model parameters. The error bars on the inverted exposure ages are ±2σ as presented in Table 3 (all results presented in the Supplementary Table A4).

6. Discussion

Our results from the Mer de Glace glacier have allowed to validate, over post-LIA timescales (i.e. over 2-137 years), the assumption that the longer a rock surface has been exposed to daylight, the deeper the luminescence signal has been bleached (Polikreti et al., 2002; 2003; Sohbati et al., 2011; 2012). Using the mathematical model propose by Sohbati et al. (2011), we accurately describe the time evolution of luminescence within a rock column. The different combinations of samples used to calibrate the model give parameter values ($\overline{\sigma\varphi}_0$ and μ) that are on the same order of magnitude for samples within similar regions and lithology, and which agree with literature values (Sohbati et al., 2011; 2012a,b).

We also observe that the evolution of luminescence signals with both time and depth within bedrock is mainly controlled by rock characteristics (lithology, texture, weathering and mineral composition). These rock properties will govern the light attenuation and penetration into rocks (parameter μ in Eq. 4), and thus the net bleaching effect on the luminescence signal. At the regional scale, the lithology should preferably be uniform to enable model calibration on some known-age surfaces (through independent dating) before application to reconstruct the exposure history of other bedrock surfaces with unknown exposure age. We see that in a granitic rock, comprising coarse quartz and feldspar grains (translucent minerals), the luminescence-bleaching front will propagate much faster than in gneiss bedrock.

Our inversion approach to constrain rock surface exposure ages from OSL data, reveals that the number of calibration samples is critical for constraining the model parameters and thus obtaining accurate exposure ages. Fortunately, calibration rock surfaces in periglacial environments can often be found from historical or remote-sensing paleo-glacier reconstructions. Other types of bedrock surfaces can be used for independent constraint, e.g. anthropogenic structures such as road-cut outcrops (e.g. Sohbati et al., 2012a) or landslide scars. The combined investigation of OSL systems with other surface exposure dating methods such as terrestrial *in situ* cosmogenic nuclides will also enable us to quantitatively assess the method's accuracy over longer timescales such as the late Pleistocene.

Experimental luminescence data presented in Figure 8 confirms that each individual sample's exposure history has been recorded in its luminescence depth profile. For the six bedrock surfaces studied here, each luminescence profile exhibits a fully-bleached signal at shallow depth (i.e. from 1 to 7 mm depending on both the exposure age and lithology, Fig. 9), followed by a sharp transition to a plateau of intensity deeper into the rock. These simple and homogeneous luminescence profiles can be compared with complex profiles previously observed following multi-stage exposure histories obtained from buried cobbles (Freiesleben et al., 2015; Sohbati et al., 2015). This confirms that the glacially-polished surfaces we sampled along the Montenvers cross-sections have experienced a simple exposure history. Furthermore, field evidence for surface preservation with glacial features (striations, flutes) indicate that the bedrock surfaces have been eroded and polished by subglacial processes before deglaciation. Weathering or mechanical erosion may lead to an underestimation of the true exposure age. Thereby, the inferred exposure history from these well-preserved rock surfaces can be used to reconstruct the paleo-glacier thickness and extent since the LIA.

Bleaching of the OSL signal has occurred at less than 1 cm depth below the exposed surface after more than 137 years of daylight exposure, highlighting the high temporal resolution of this novel method for paleo-glacier reconstruction. In mountainous locations such as the Mont Blanc massif, where the glacial history has been complex with several glacier fluctuations during the late Pleistocene to Holocene (recurrent retreat/advance cycles; e.g. LeRoy et al., 2015), the application of absolute dating methods such as terrestrial *in situ* cosmogenic nuclides are difficult due to potential inheritance from previous exposure events (e.g. Goehring et al., 2011). One of the main advantages of OSL surface exposure dating is that daylight bleaching of the OSL signal occurs within the first few millimetres below the exposed rock surface. Short glacier re-advances over the late Holocene (e.g. LeRoy et al., 2015) would have easily eroded the first centimetres of bedrock, consequently resetting the OSL system before the post-LIA glacier retreat. We have thus shown in this study that well-preserved polished bedrock surfaces can be used for the application of OSL surface exposure dating in order to constrain the timing of the last glacial retreat from the LIA to present day, improving our temporal resolution for glacier reconstruction. Over such timescales, the contribution of the trap filling rate ($F(x)$ in Section 2.3) from radioactive decay in gneissic or granitic rock can be assumed to be negligible (see Supplementary material A2). However, this contribution may have to be taken into account when extending paleo-glacier reconstruction using OSL surface exposure dating to longer timescales, e.g. since the Last Glacial Maximum or further back into the Quaternary. Over the same timescales, weathering and erosion of the surface are likely to play a significant role.

7. Conclusions

In this study, we have investigated the potential of OSL surface exposure dating for quantitatively reconstructing post-LIA glacier retreat. We worked along an altitudinal cross-section of the Mer de Glace glacier (Mont Blanc massif, France), and collected glacially-polished bedrock surfaces with known exposure ages (from 3 to 137 years) along the Montenvers profile from around 1841 m.a.s.l. elevation to the present-day glacier position (1696 m.a.s.l.). We have developed a statistical approach to calibrate the bleaching model parameters from known-age samples. Experimental IRSL depth-profile data for five different polished bedrock surfaces show an increase of the luminescence signal bleaching depth with exposure age. We conclude that OSL surface exposure dating can be applied to glacial and periglacial environments, and is a promising tool for high-resolution reconstruction of recent ice-extent and thickness fluctuations, both in space and time. However, we find that several calibration samples must be used to calibrate the model parameters before inferring exposure ages on bedrock surfaces within a specific area, taking into account the potential variation in bedrock lithology. We also find that measurement uncertainties, intrinsic data noise or both can result in large uncertainties on inverted ages, especially when applying this method over 10^3-10^4 yr timescales.

Acknowledgements

We thank N. Brown and an anonymous reviewer for constructive and helpful comments. This work was supported by the Swiss National Science Foundation (SNFS) funded Swiss-AlpArray SINERGIA project (CRSII2_154434/1). PGV acknowledges support from SNFS grants PZ00P2_148191 and PP00P2_170559, and GEK from SNFS grant PZ00P2-167960. The authors would like to thank the French glacier observatory GLACIOCLIM (http://www-lgge.ujf-grenoble.fr/ServiceObs/index.htm) for providing their data. We are grateful to S. Coutterand, M. Delasoie, A. Licul, N. Stalder and V. Višnjević for fieldwork support; M. Faria and K. Häring for laboratory support.

References

Aitken, M.J., 1985. Thermoluminescence dating. Academic press.

Aitken, M.J., 1998. An Introduction to Optical Dating The Dating of Quaternary: Sediments by the Use of Photon-stimulated Luminescence. Oxford University press.

Bailey, R.M., 2004. Paper I-simulation of dose absorption in quartz over geological timescales and its implications for the precision and accuracy of optical dating. Radiation Measurements 38, 299-310.

Baillie M.G.L., 1995. A Slice Through Time: dendrochronology and precision dating. London, Routledge, 176 p.

Balco, G., 2011. Contributions and unrealized potential contributions of cosmogenic nuclide exposure dating to glacier chronology, 1990-2010. Quaternary Science Reviews 30, 3-27.

Bini, A., Buoncristiani, J.F., Couterrand, S., Ellwanger, D., Felber, M., Florineth, D., Graf, H.R., Keller, O., Kelly, M., Schlüchter, C., Schoeneich, P., 2009. Switzerland during the Last Glacial Maximum 1: 500,000. Bundesamt für Landestopografie swisstopo.

Blumthaler, M., Ambach, W., Ellinger, R., 1997. Increase in solar UV radiation with altitude. Journal of Photochemistry and Photobiology B: Biology 39, 130-134.

Bøtter-Jensen, L., Thomsen, K.J., Jain, M., 2010. Review of optically stimulated luminescence (OSL) instrumental developments for retrospective dosimetry. Radiation Measurements 45, 253-257.

Broecker, W., Denton, G., 1990. What drives glacial cycles? Scientific American 262, 43-50.

Brown, N.D., Rhodes, E.J., Harrison, T.M., 2017. Using thermoluminescence signals from feldspars for low-temperature thermochronology. Quaternary Geochronology 42, 31-41.

Coutterand, S., Buoncristiani, J.-F., 2006. Paléogéographie du dernier maximum glaciaire du Pléistocène récent de la région du massif du Mont Blanc, France. Quaternaire. Revue de l'Association française pour l'étude du Quaternaire 17, 35-43.

Dobmeier, C., 1998. Variscan P–T deformation paths from the southwestern Aiguilles Rouges massif (External massif, western Alps) and their implication for its tectonic evolution. Geologische Rundschau 87, 107-123.

Duller GAT. 2005. Luminescence Analyst. University of Wales: Aberystwyth.

Duller, G.A.T., 2008. Single-grain optical dating of Quaternary sediments: why aliquot size matters in luminescence dating. Boreas 37, 589-612.

Egholm, D., Nielsen, S., Pedersen, V.K., Lesemann, J.-E., 2009. Glacial effects limiting mountain height. Nature 460, 884-887.

Ehlers, J., Gibbard, P.L., 2007. The extent and chronology of Cenozoic Gobal Glaciation. Quaternary International 164-165, 6-20.

Freiesleben, T., Sohbati, R., Murray, A., Jain, M., Al Khasawneh, S., Hvidt, S., Jakobsen, B., 2015. Mathematical model quantifies multiple daylight exposure and burial events for rock surfaces using luminescence dating. Radiation Measurements 81, 16-22.

Fuchs, M., Owen, L.A., 2008. Luminescence dating of glacial and associated sediments: review, recommendations and future directions. Boreas 37, 636-659.

Gardent, M., Rabatel, A., Dedieu, J.-P., Deline, P., 2014. Multitemporal glacier inventory of the French Alps from the late 1960s to the late 2000s. Global and Planetary Change 120, 24-37.

Goehring, B.M., Schaefer, J.M., Schluechter, C., Lifton, N.A., Finkel, R.C., Jull, A.T., Akçar, N., Alley, R.B., 2011. The Rhone Glacier was smaller than today for most of the Holocene. Geology 39, 679-682.

Goehring, B.M., Vacco, D.A., Alley, R.B., Schaefer, J.M., 2012. Holocene dynamics of the Rhone Glacier, Switzerland, deduced from ice flow models and cosmogenic nuclides. Earth and Planetary Science Letters 351, 27-35.

Guralnik, B., Jain, M., Herman, F., Ankjærgaard, C., Murray, A.S., Valla, P.G., Preusser, F., King, G.E., Chen, R., Lowick, S.E., 2015. OSL-thermochronometry of feldspar from the KTB borehole, Germany. Earth and planetary science letters 423, 232-243.

Habermann, J., Schilles, T., Kalchgruber, R., Wagner, G.A., 2000. Steps towards surface dating using luminescence. Radiation Measurements 32, 847-851.

Hajdas, I., 2008. Radiocarbon dating and its applications in Quaternary studies. Eiszeitalter und Gegenwart Quaternary Science Journal 57, 24.

Herbert, T.D., Lawrence, K.T., Tzanova, A., Peterson, L.C., Caballero-Gill, R., Kelly, C.S., 2016. Late Miocene global cooling and the rise of modern ecosystems. Nature Geosci 9, 843-847.

Hippe, K., Ivy-Ochs, S., Kober, F., Zasadni, J., Wieler, R., Wacker, L., Kubik, P.W., Schlüchter, C., 2014. Chronology of Lateglacial ice flow reorganization and deglaciation in the Gotthard Pass area, Central Swiss Alps, based on cosmogenic ^{10}Be and in situ ^{14}C. Quaternary Geochronology 19, 14-26.

Huntley, D.J., Godfrey-Smith, D.I., Thewalt, M.L., 1985. Optical dating of sediments. Nature 313, 105-107.

Ivy-Ochs, S., 2015. Glacier variations in the European Alps at the end of the last glaciation. Cuadernos de investigación geográfica 41, 295-315.

Ivy-Ochs, S., Kerschner, H., Reuther, A., Maisch, M., Sailer, R., Schaefer, J., Kubik, P.W., Synal, H.-A., Schlüchter, C., 2006. The timing of glacier advances in the northern European Alps based on surface exposure dating with cosmogenic 10Be, 26Al, 36Cl, and 21Ne. Geological Society of America Special Papers 415, 43-60.

Ivy-Ochs, S., Kerschner, H., Maisch, M., Christl, M., Kubik, P.W., Schlüchter, C., 2009. Latest Pleistocene and Holocene glacier variations in the European Alps. Quaternary Science Reviews 28, 2137-2149.

Ivy-Ochs, S., Briner, J.P., 2014. Dating disappearing ice with cosmogenic nuclides. Elements 10, 351-356.

King, G., Herman, F., Lambert, R., Valla, P., Guralnik, B., 2016. Multi-OSL-thermochronometry of feldspar. Quaternary Geochronology 33, 76-87.

Lal, D., 1991. Cosmic ray labeling of erosion surfaces: in situ nuclide production rates and erosion models. Earth and Planetary Science Letters 104, 424-439.

Lang, A., Hönscheidt, S., 1999. Age and source of colluvial sediments at Vaihingen-Enz, Germany. Catena 38, 89-107.

Laskaris, N., Liritzis, I., 2011. A new mathematical approximation of sunlight attenuation in rocks for surface luminescence dating. Journal of Luminescence 131, 1874-1884.

Le Roy, M., Nicolussi, K., Deline, P., Astrade, L., Edouard, J.-L., Miramont, C., Arnaud, F., 2015. Calendar-dated glacier variations in the western European Alps during the Neoglacial: the Mer de Glace record, Mont Blanc massif. Quaternary Science Reviews 108, 1-22.

Lean, J., 1987. Solar Ultraviolet Irradiance Variations: A review. Journal of Geophysical Research 92,839-968.

Liritzis, I., 1994. A new dating method by thermoluminescence of carved megalithic stone building. Comptes rendus de l'Académie des sciences. Série 2. Sciences de la terre et des planètes 319, 603-610.

Liritzis, I., 2011. Surface dating by luminescence: an overview. Geochronometria 38, 292-302.

Molnar, P., England, P., 1990. Late Cenozoic uplift of mountain ranges and global climate change: chicken or egg? Nature 346, 29-34.

Murray, A.S., Wintle, A.G., 2000. Luminescence dating of quartz using an improved single-aliquot regenerative-dose protocol. Radiation measurements 32, 57-73.

Nussbaumer, S., Zumbühl, H.J., Steiner, D., 2007. Fluctuations of the Mer de glace (Mont Blanc area, France) AD 1500-2050. An interdisciplinary approach using new historical data and neural network simulations. Zeitschrift für Gletscherkunde und Glazialgeologie ZGG, 5-175.

Peizhen, Z., Molnar, P., Downs, W.R., 2001. Increased sedimentation rates and grain sizes 2–4 Myr ago due to the influence of climate change on erosion rates. Nature 410, 891-897.

Penck, A., 1905. Glacial features in the surface of the Alps. The Journal of Geology 13, 1-19.

Preusser, F., Graf, H.R., Keller, O., Krayss, E., Schlüchter, C., 2011. Quaternary glaciation history of northern Switzerland. Quaternary Science Journal 60(2-3), 282-305.

Polikreti, K., Michael, C., Maniatis, Y., 2002. Authenticating marble sculpture with thermoluminescence. Ancient TL 20, 11-18.

Polikreti, K., Michael, C., Maniatis, Y., 2003. Thermoluminescence characteristics of marble and dating of freshly excavated marble objects. Radiation Measurements 37, 87-94.

Rabatel, A., Letréguilly, A., Dedieu, J., Eckert, N., 2013. Changes in glacier equilibrium-line altitude in the western Alps from 1984 to 2010: evaluation by remote sensing and modeling of the morpho-topographic and climate controls. Cryosphere 7, p. 1455-p. 1471.

Rhodes, E.J., 2011. Optically stimulated luminescence dating of sediments over the past 200,000 years. Annual Review of Earth and Planetary Sciences 39, 461-488.

Richards, M.P., 1994. Luminescence dating of quartzite from the Diring Yuriakh site. M.A. Thesis, Simon Fraser University, unpublished.

Schimmelpfennig, I., Schaefer, J.M., Akçar, N., Koffman, T., Ivy-Ochs, S., Schwartz, R., Finkel, R.C., Zimmerman, S., Schlüchter, C., 2014. A chronology of Holocene and Little Ice Age glacier culminations of the Steingletscher, Central Alps, Switzerland, based on high-sensitivity beryllium-10 moraine dating. Earth and Planetary Science Letters 393, 220-230.

Simms, A.R., DeWitt, R., Kouremenos, P., Drewry, A.M., 2011. A new approach to reconstructing sea levels in Antarctica using optically stimulated luminescence of cobble surfaces. Quaternary Geochronology 6, 50-60.

Simkins, L.M., Simms, A.R., DeWitt, R., 2013. Relative sea-level history of Marguerite Bay, Antarctic Peninsula derived from optically stimulated luminescence-dated beach cobbles. Quaternary Science Reviews 77, 141-155.

Singarayer, J.S., 2002. Linearly modulated optically stimulated luminescence of sedimentary quartz: Physical mechanisms and implications for dating. D.Phil. thesis, University of Oxford. 345 pp.

Sohbati, R., Murray, A., Jain, M., Buylaert, J.-P., Thomsen, K., 2011. Investigating the resetting of OSL signals in rock surfaces. Geochronometria 38, 249-258.

Sohbati, R., Jain, M., Murray, A., 2012a. Surface exposure dating of non-terrestrial bodies using optically stimulated luminescence: A new method. Icarus 221, 160-166.

Sohbati, R., Murray, A.S., Buylaert, J.-P., Almeida, N.A.C., Cunha, P.P., 2012b. Optically stimulated luminescence (OSL) dating of quartzite cobbles from the Tapada do Montinho archaeological site (east-central Portugal). Boreas 41, 452-462.

Sohbati, R., Murray, A., Porat, N., Jain, M., Avner, U., 2015. Age of a prehistoric "Rodedian" cult site constrained by sediment and rock surface luminescence dating techniques. Quaternary Geochronology 30, 90-99.

Theocaris, P., Liritzis, I., Galloway, R., 1997. Dating of two Hellenic pyramids by a novel application of thermoluminescence. Journal of Archaeological Science 24, 399-405.

Vafiadou, A., Murray, A., Liritzis, I., 2007. Optically stimulated luminescence (OSL) dating investigations of rock and underlying soil from three case studies. Journal of Archaeological Science 34, 1659-1669.

Valla, P.G., Lowick, S.E., Herman, F., Champagnac, J.-D., Steer, P., Guralnik, B., 2016. Exploring $IRSL_{50}$ fading variability in bedrock feldspars and implications for OSL thermochronometry. Quaternary Geochronology 36, 55-66.

Vincent, C., Harter, M., Gilbert, A., Berthier, E., Six, D., 2014. Future fluctuations of Mer de Glace, French Alps, assessed using a parameterized model calibrated with past thickness changes. Annals of Glaciology 55, 15-24.

Wirsig, C., Zasadni, J., Ivy-Ochs, S., Christl, M., Kober, F., Schlüchter, C., 2016. A deglaciation model of the Oberhasli, Switzerland. Journal of Quaternary Science 31, 46-59.

Wintle, A.G., Murray, A.S., 2006. A review of quartz optically stimulated luminescence characteristics and their relevance in single-aliquot regeneration dating protocols. Radiation Measurements 41, 369-391.

Zachos, J.C., Shackleton, N.J., Revenaugh, J.S., Pälike, H., Flower, B.P., 2001. Climate response to orbital forcing across the Oligocene-Miocene boundary. Science 292, 274-278.

Supplementary Material

A1. Ice surface reconstruction

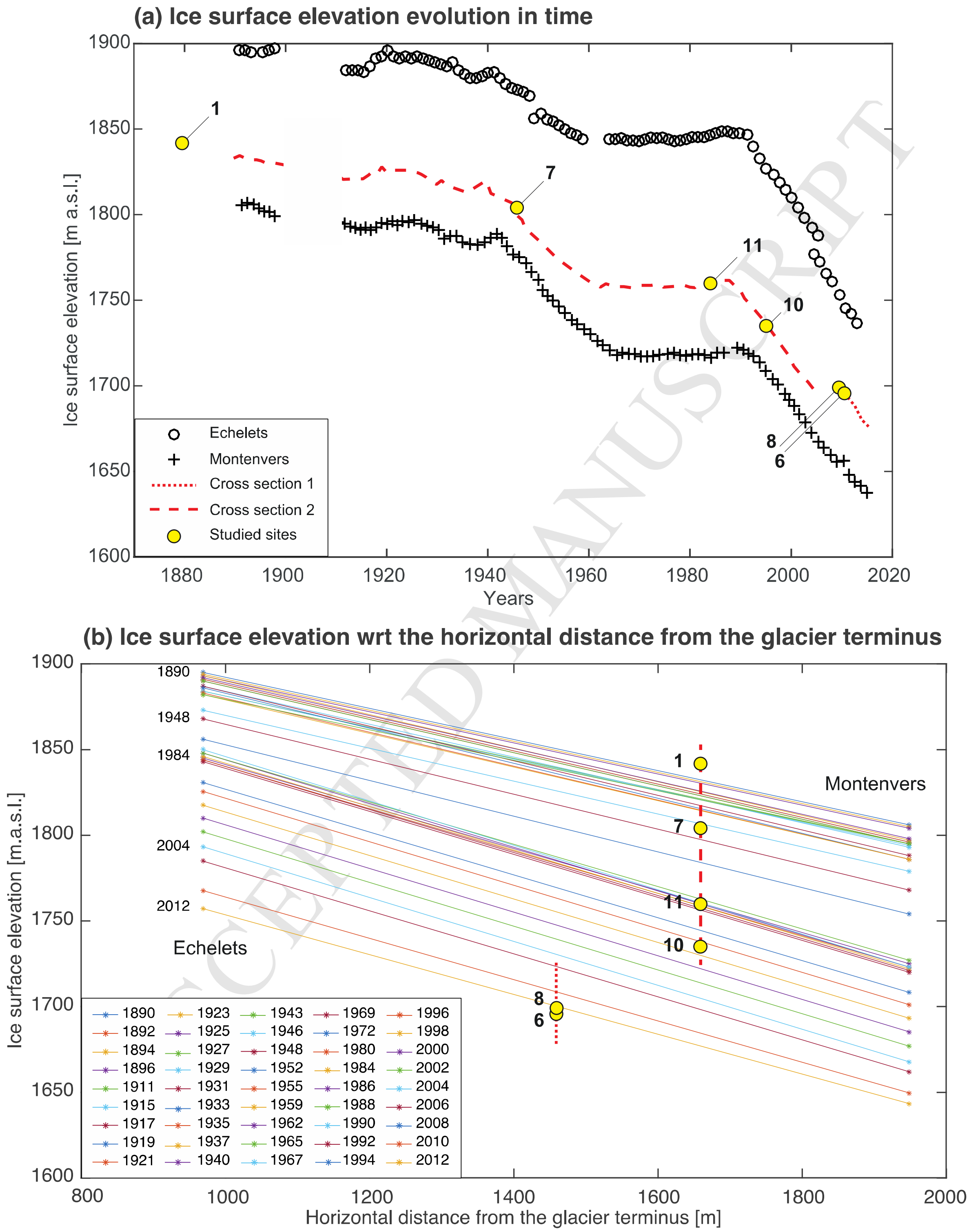

Figure A1: (a) Reconstruction of averaged ice-surface elevation [m.a.s.l.] through time along the Mer de Glace glacier (see locations of cross-sections on Fig.1). Averaged ice-surface elevations at the Montenvers (crosses) and Echelets (circles) cross-sections. The cross-sections 1 and 2 (red dashed lines) have been interpolated from the Montenvers and Echelets cross-sections, and used to project the studied samples (yellow circles). (b) Ice-surface elevation with respect to the horizontal distance from the glacier terminus used for the interpolation of the Montenvers and Echelets cross-sections. The ice surface elevations have been reconstructed from historical maps, survey reports and aerial photogrammetry (modified from Vincent et al., 2014). The dataset was kindly provided by the French glacier observatory GLACIOCLIM (http://www-lgge.ujf-grenoble.fr/ServiceObs/index.htm).

A2. Dose rate sensitivity

The sensitivity of luminescence signal evolution to the dose rate is tested after four different daylight exposure times (1, 10, 100 and 1000 years of exposure), with a null dose rate and an extremely high dose rate ($\dot{D} \approx 14$ Gy ka^{-1}, King et al., 2016). We used an equation developed by Sohbati et al. (2012) describing the luminescence evolution $L(x)$ as a function of the exposure time t [s], depth x [mm], charge detrapping rate $\overline{\sigma\varphi}_0$ [s^{-1}], attenuation factor μ [mm^{-1}], a sample-dependent constant that characterises filling rate D_0 [Gy] and the natural dose rate $\dot{D}$ [Gy s^{-1}].

$$L(x) = \frac{\overline{\sigma\varphi}_0\, e^{-\mu x} e^{-t\left[\overline{\sigma\varphi}_0\, e^{-\mu x} + \frac{\dot{D}(x)}{D_0}\right]} + \frac{\dot{D}(x)}{D_0}}{\overline{\sigma\varphi}_0\, e^{-\mu x} + \frac{\dot{D}(x)}{D_0}} \quad \text{(A1)}$$

The resulting comparison shows that the luminescence signal is not sensitive to dose rate over millenial timescales. We thus consider the dose rate as negligible for our applications of OSL surface exposure dating, and do not take it into account in the luminescence evolution equation.

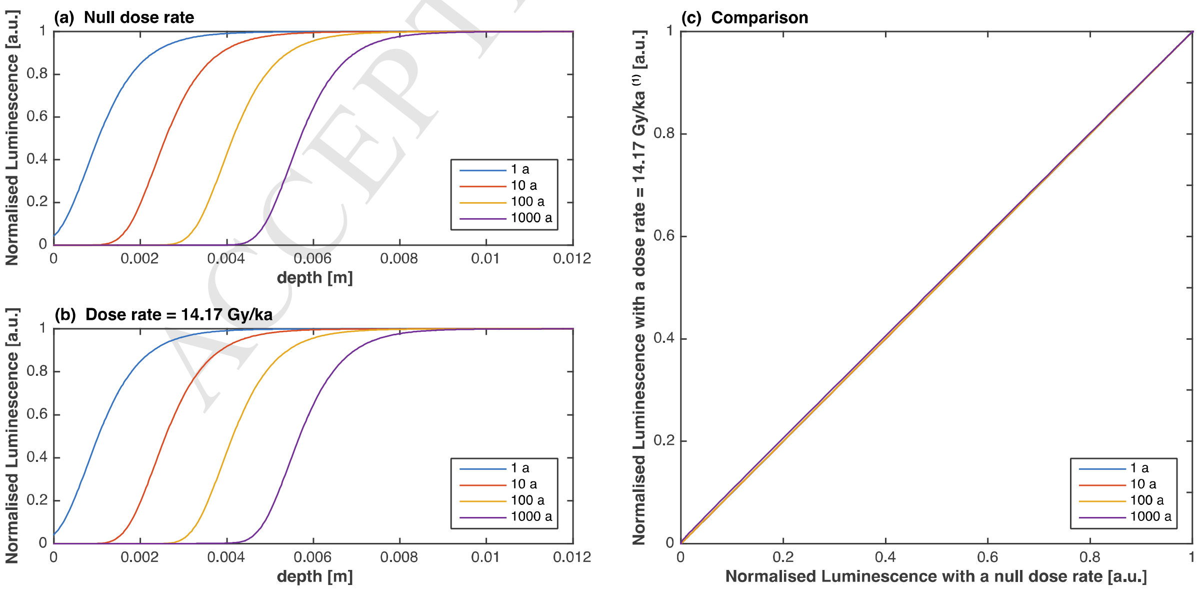

Figure A2: Evolution of the nomalised luminescence signal through time and depth for 1, 10, 100 and 1000 years of daylight exposure, taking into account (a) a null dose rate and (b) an extremely high dose rate of ~14 Gy/ka (King et al., 2016). Inset (c) shows the comparison between the result with two different dose rates.

A3. Luminescence measurement tests

The purpose of the following tests is to find the most appropriate infrared stimulated luminescence (IRSL) measurement conditions for analysis of the collected samples from the Montenvers site. We first performed a residual dose determination. Under natural daylight conditions, luminescence signals of feldspar may not be completely reset, leaving a residual dose. The residual test allows the evaluation of this remaining natural dose (which may also originate from other sources e.g. thermal transfer). We first reset the luminescence signal by exposing rock slices (3 slices for a representative sample of Montenvers site) to daylight for about 3 hours before analysing both slide sides. We then measured the residual dose using infrared stimulation at 50°C ($IRSL_{50}$) following different preheat temperatures (during 60 s). The residual dose after a preheat temperature of 250°C is 0.25 ± 0.45 Gy. With preheat temperature equal to 275°C, the residual dose is 0.85 ± 0.43 Gy. For preheat temperature equal to 300°C and 325°C, the residual doses increase to 2.94 ± 0.41 Gy and 2.10 ± 0.52 Gy respectively.

We then proceeded to a dose recovery test with preheat-plateau to determine the most appropriate preheat temperature. Thereby we quantified the recovered doses with $IRSL_{50}$ for the same range of preheat temperatures explored in the residuals test. We analyzed 3 rock slices with a laboratory beta dose of 27.25 Gy after complete optical bleaching (both disk sides exposed to daylight for about 3 hours). The samples were not heated prior the daylight bleaching. Preheat temperatures 250°C, 275°C, 300°C, 325°C were investigated, and results are corrected for the residual dose values reported in Table A1. For preheat temperatures of 250°C, 275°, 300°C and 325°C, we obtained dose recovery ratios of 0.90 ± 0.10, 0.87 ± 0.17, 0.77 ± 0.23 and 0.85 ± 0.15, respectively (Table A1). The optimal preheat temperature for both the residual dose and dose recovery is thus 250°C, and was used in all subsequent experiments.

Table A1: Results of the residual test and the dose recovery preheat plateau test after a given beta dose of 27.25 Gy.

Preheat Temperature (°C)	250	275	300	325
Residual dose (Gy)	0.25 ± 0.45	0.85 ± 0.43	2.94 ± 0.41	2.1 ± 0.52
Dose recovery ratio	0.9 ± 0.10	0.87 ± 0.17	0.77 ± 0.23	0.85 ± 0.15

Table A2: Sensitivity corrected luminescence signal intensities with depth. The depth *x* (cm) is measured during core slicing with a high-precision numerical micrometre. IRSL measurements

(*Lx/Tx)* are the results of the luminescence analysis (as explained in Section 4) and the analytical error on the measurement (*Lx/Tx err.)* is calculated in Analyst v.4.31.7 including a measurement error of 1.5%. Note: Each line corresponds to the measurement of one single rock slice.

MBMV1		
x [cm]	Lx/Lx	Lx/Tx err.
1.6	0.00	0.000
2.6	0.01	0.000
3.6	0.34	0.007
4.7	0.60	0.013
5.7	0.86	0.018
6.7	0.92	0.020
7.7	1.04	0.022
8.6	0.97	0.021
9.5	0.97	0.021
10.4	1.00	0.021
11.4	1.05	0.022
12.4	1.12	0.024
13.5	0.95	0.020
14.5	0.98	0.021
15.4	1.01	0.021
16.4	0.98	0.021
17.6	0.94	0.020
1.7	0.01	0.000
2.8	0.01	0.000
3.8	0.05	0.001
4.8	0.34	0.007
5.8	0.64	0.014
6.8	0.97	0.021
7.8	1.02	0.022
8.9	0.94	0.020
10.0	1.07	0.023
2.3	0.03	0.001
3.4	0.21	0.005
4.4	0.66	0.014
5.4	0.86	0.018
6.4	0.96	0.020
7.3	1.08	0.023
8.3	1.01	0.021
9.2	1.10	0.023
10.2	1.00	0.021
11.2	0.96	0.020
12.3	0.88	0.019
13.2	0.88	0.019
14.2	0.97	0.021
15.2	0.90	0.019

MBMV6		
x [cm]	Lx/Lx	Lx/Tx err.
1.3	0.00	0.000
2.4	0.00	0.000
3.4	0.00	0.000
4.5	0.04	0.001
5.5	0.15	0.003
6.5	0.70	0.015
7.5	0.91	0.019
8.5	0.92	0.020
9.5	0.99	0.021
10.5	1.01	0.021
11.5	1.03	0.022
12.5	1.13	0.024
13.5	1.10	0.023
14.5	1.03	0.022
2.4	0.01	0.000
3.3	0.02	0.000
4.4	0.12	0.002
5.4	0.45	0.009
6.4	0.75	0.016
7.4	0.88	0.019
8.4	1.10	0.023
9.4	1.06	0.022
10.4	0.92	0.020
11.4	0.96	0.020
12.4	0.86	0.018
13.4	0.90	0.019
14.3	1.09	0.023
15.2	1.09	0.023
1.4	0.01	0.000
2.2	0.01	0.000
3.0	0.15	0.003
3.9	0.31	0.007
4.7	0.70	0.015
6.3	0.93	0.020
7.1	0.82	0.017
7.9	0.89	0.019
8.6	0.89	0.019
9.4	0.79	0.017

MBMV7		
x [cm]	Lx/Lx	Lx/Tx err.
2.3	0.01	0.000
3.3	0.11	0.002
4.4	0.99	0.021
5.4	1.06	0.023
6.4	1.06	0.022
7.4	1.03	0.022
8.4	0.95	0.020
9.3	0.94	0.020
10.3	0.95	0.020
11.4	0.92	0.020
12.4	0.94	0.020
1.7	0.01	0.000
2.8	0.03	0.001
3.7	0.42	0.009
4.5	0.79	0.017
5.5	0.84	0.018
6.5	0.97	0.021
7.5	1.15	0.024
8.6	0.94	0.020
9.6	1.08	0.023
10.7	1.12	0.024
11.8	0.97	0.021
1.6	0.00	0.000
2.8	0.04	0.001
3.8	0.42	0.009
4.8	0.95	0.020
5.9	1.06	0.022
6.9	1.08	0.023
8.0	0.92	0.020
8.9	1.07	0.023
10.0	0.94	0.020
11.3	0.94	0.020
12.4	1.00	0.021

MBMV8		
x [cm]	Lx/Lx	Lx/Tx err.
1.5	0.31	0.007
2.8	0.62	0.013
3.9	0.92	0.020
5.0	1.04	0.022
6.1	0.96	0.020
7.1	0.99	0.021
8.2	1.00	0.021
9.2	1.08	0.023
10.3	1.10	0.023
11.4	1.12	0.024
12.4	1.01	0.021
2.0	0.39	0.008
3.0	0.96	0.020
4.0	0.89	0.037
7.0	1.05	0.022
8.0	0.95	0.020
9.0	1.04	0.022
10.1	1.15	0.024
11.1	1.07	0.023
12.2	0.91	0.019
13.2	1.01	0.021
1.8	0.85	0.018
2.9	0.93	0.020
4.2	1.01	0.022
5.4	0.90	0.019
6.6	0.94	0.020
7.6	1.06	0.023
8.6	0.93	0.020
9.7	1.00	0.021
10.7	1.06	0.023
12.1	1.04	0.022
13.4	0.84	0.018

MBMV10		
x [cm]	Lx/Lx	Lx/Tx err.
2.4	0.42	0.009
3.6	0.76	0.016
4.7	1.05	0.022
5.6	0.91	0.019
6.7	1.05	0.022
7.8	1.12	0.024
8.7	0.88	0.019
9.8	0.98	0.021
10.9	1.14	0.024
11.9	0.96	0.020
13.0	0.93	0.020
3.1	0.80	0.017
4.2	0.96	0.020
5.3	1.06	0.023
6.4	1.10	0.023
7.4	0.97	0.021
8.4	0.94	0.020
9.4	0.91	0.019
10.6	0.98	0.021
11.7	0.87	0.018
12.7	1.04	0.022
13.7	1.04	0.022
1.8	0.02	0.000
3.1	0.23	0.005
4.2	0.73	0.015
5.3	1.09	0.023
6.4	0.93	0.020
7.4	1.00	0.021
8.5	0.93	0.020
9.7	1.07	0.023
10.8	0.96	0.021

MBMV11		
x [cm]	Lx/Lx	Lx/Tx err.
2.2	0.00	0.000
3.3	0.01	0.000
4.2	0.27	0.006
5.2	0.62	0.013
6.1	0.86	0.019
7.1	1.05	0.022
8.0	0.97	0.021
9.0	0.80	0.017
9.9	0.93	0.020
10.8	0.89	0.019
11.8	0.84	0.018
12.7	0.88	0.019
2.1	0.10	0.002
3.2	0.80	0.017
4.2	0.82	0.018
5.1	0.88	0.019
6.1	1.04	0.022
7.0	0.96	0.021
8.0	0.99	0.021
8.9	0.92	0.020
9.8	0.98	0.021
11.7	0.92	0.020
12.7	0.91	0.020
1.8	0.01	0.000
2.8	0.21	0.005
3.8	0.60	0.013
4.7	0.86	0.018
5.7	0.96	0.021
6.7	0.97	0.021
7.7	0.90	0.019
8.7	0.94	0.020
9.6	1.04	0.022
10.6	1.21	0.026
11.5	1.00	0.021
12.4	0.93	0.020
1.9	0.03	0.001
3.2	0.15	0.003
4.1	0.53	0.011
5.1	0.99	0.021
6.1	1.05	0.022
7.0	1.1	0.024
7.9	1.2	0.026
8.8	1.0	0.022
9.8	1.1	0.024
10.7	1.2	0.026
11.6	1.1	0.024
12.6	0.9	0.019

Table A3: Best-fit values of $\overline{\sigma\varphi}_0$ and μ determined for each sample, calculated from combinations of three and four samples.

Calibration				$\overline{\sigma\varphi}_0$ [s^{-1}]			μ [mm^{-1}]		
combination				Best-fit	+1σ	-1σ	Best-fit	+1σ	-1σ
with 3 samples, MBMV...									
1	7	8		$1.2\ 10^{-7}$	$1.2\ 10^{-7}$	$1.1\ 10^{-7}$	1.51	1.52	1.50
1	7	10		$6.6\ 10^{-8}$	$7.6\ 10^{-8}$	$6.4\ 10^{-8}$	1.42	1.43	1.38
1	7	11		$9.4\ 10^{-8}$	$9.6\ 10^{-8}$	$7.8\ 10^{-8}$	1.42	1.45	1.39
1	8	11		$7.4\ 10^{-8}$	$7.5\ 10^{-8}$	$6.1\ 10^{-8}$	1.39	1.39	1.34
1	8	10		$1.0\ 10^{-7}$	$1.0\ 10^{-7}$	$1.0\ 10^{-7}$	1.42	1.43	1.41
1	10	11		$6.6\ 10^{-8}$	$8.3\ 10^{-8}$	$6.0\ 10^{-8}$	1.39	1.39	1.33
7	8	10		$1.3\ 10^{-7}$	$1.3\ 10^{-7}$	$1.3\ 10^{-7}$	1.58	1.58	1.56
7	8	11		$1.2\ 10^{-7}$	$1.2\ 10^{-7}$	$1.2\ 10^{-7}$	1.51	1.52	1.50
7	10	11		$1.4\ 10^{-7}$	$1.5\ 10^{-7}$	$1.3\ 10^{-7}$	1.58	1.60	1.55
8	10	11		$8.1\ 10^{-8}$	$9.1\ 10^{-8}$	$7.3\ 10^{-8}$	1.34	1.37	1.31
with 4 samples, MBMV…									
1	7	8	10	$9.5\ 10^{-8}$	$9.9\ 10^{-8}$	$8.5\ 10^{-8}$	1.48	1.48	1.45
1	7	8	11	$1.1\ 10^{-7}$	$1.1\ 10^{-7}$	$1.1\ 10^{-7}$	1.48	1.49	1.47
1	7	10	11	$7.4\ 10^{-8}$	$8.1\ 10^{-8}$	$6.5\ 10^{-8}$	1.38	1.41	1.36
1	8	11	10	$9.0\ 10^{-8}$	$9.4\ 10^{-8}$	$8.7\ 10^{-8}$	1.42	1.42	1.40
7	10	11	8	$1.2\ 10^{-7}$	$1.2\ 10^{-7}$	$1.2\ 10^{-7}$	1.53	1.53	1.52

Table A4: Inversion results for exposure age using the different calibration combinations of bedrock samples. Grey shading shows the inverted results for a specific sample when not included in the calibration combination (i.e. the exposure age of the specific sample has not used for the calibration of the model). These results are used to produce Figures 10c-d.

Calibration				MBMV1 - 137 yrs				MBMV7 - 69 yrs				MBMV8 - 3 yrs				MBMV10 - 18 yrs				MBMV11 - 30 yrs			
combination				Best fit	Median	+2 σ	-2 σ	Best fit	Median	+2 σ	-2 σ	Best fit	Median	+2 σ	-2 σ	Best fit	Median	+2 σ	-2 σ	Best fit	Median	+2 σ	-2 σ
Individually				146	152	172	126	89	79	88	67	2	3	3	2	19	19	23	14	50	42	50	34
with all the sample excluding MBMV6				164	161	185	132	61	63	68	57	3	3	4	3	17	14	18	9	62	57	70	41
with 3 samples, MBM V...																							
1	7	8		184	166	190	136	56	62	67	56	3	3	3	2	9	13	17	9	53	54	69	40
1	7	10		194	183	213	146	77	80	88	71	5	5	5	4	21	18	23	13	90	69	88	50
1	7	11		118	126	149	103	56	56	61	50	3	3	4	3	15	12	16	9	57	50	61	35
1	8	11		122	135	159	104	61	63	70	56	3	4	4	3	13	15	18	10	55	53	68	39
1	8	10		106	113	134	92	50	50	55	45	3	3	3	2	14	12	15	8	50	43	55	31
1	10	11		174	150	181	119	67	71	80	63	4	4	5	4	17	17	21	12	44	61	77	44
7	8	10		181	211	242	173	78	74	82	64	3	3	3	2	16	13	17	9	78	65	78	48
7	8	11		165	162	189	136	66	62	67	56	3	3	3	2	14	13	17	9	40	54	68	40
7	10	11		206	189	216	155	65	65	73	57	3	3	3	2	15	12	15	8	65	58	70	43
8	10	11		116	93	116	71	46	50	55	43	3	3	4	3	11	12	15	9	52	42	52	29
with 4 samples, MBMV …																							
1	7	8	10	176	170	194	139	63	67	73	61	4	4	4	3	10	15	19	10	68	61	75	43
1	7	8	11	177	152	174	125	63	59	64	54	3	3	3	3	15	13	17	9	63	52	66	38
1	7	10	11	129	129	154	98	58	62	69	54	4	4	4	3	13	14	18	10	38	52	66	38
1	8	11	10	117	134	155	106	58	58	64	52	4	3	4	3	16	13	17	9	42	52	64	36
7	10	11	8	159	168	196	141	63	63	69	56	2	3	3	2	16	13	16	9	52	55	69	41

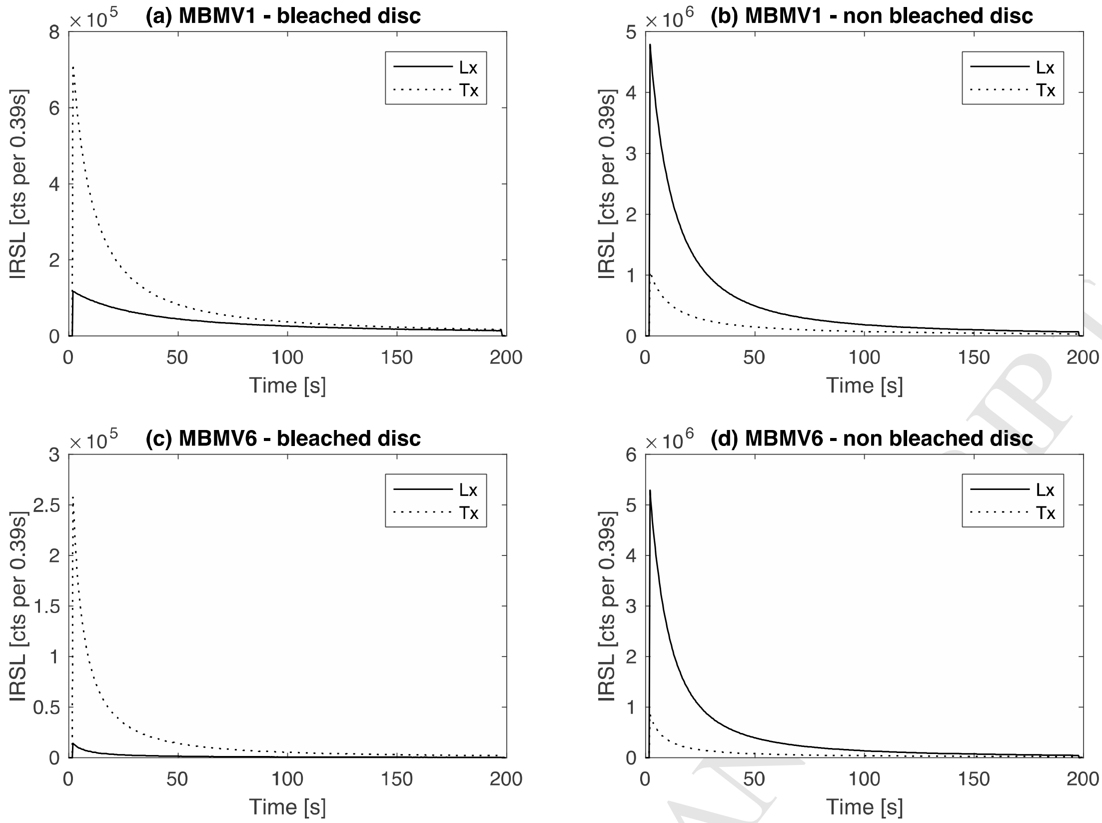

Figure A3: Natural infrared stimulated signal (solid line, Lx) and test dose (27.25 Gy) subsequent luminescence response (dashed line, Tx) for a bleached signal (surface disc) (a) and (b) and for non-bleached signal (inside core disc) (b) and (c). (a) and (b) are IRSL signal representative for gneissic lithology (sample MBMV1). (c) and (d) for granitic lithology (sample MBMV6).

References

G.E. King, F. Herman and B. Guralnik, 2016. Northward migration of the eastern Himalayan syntax revealed by OSL-thermochronometry. Science 353 (6301), 800-804.

Sohbati, R., Jain, M., Murray, A., 2012a. Surface exposure dating of non-terrestrial bodies using optically stimulated luminescence: A new method. Icarus 221, 160-166.